Pergamon

Int. J. Heat Mass Transfer. Vol. 38, No. 10, pp. 1751–1772, 1995

0017-9310/95 $9.50+0.00

0017-9310(94)00310-6

Nonlinear instability of travelling waves with a continuous spectrum

L. S. YAO and S. GHOSH MOULIC†

Department of Mechanical and Aerospace Engineering, Arizona State University, Tempe, AZ 85287-6106, U.S.A.

(*Received* 7 *June* 1994 *and in final form* 5 *October* 1994)

Abstract—The nonlinear evolution of a continuous spectrum of travelling waves resulting from the growth of unstable disturbances in fully-developed fluid flows is studied. The disturbance is represented in its most general form by a Fourier integral over all possible wavenumbers. The Fourier components of the disturbance quantities are expanded in a series of the linear-stability eigenfunctions, and a set of integro-differential equations for the amplitude density function of a continuous spectrum is derived. No approximations are involved in this reduction; hence, a numerical solution of the integro-differential equations is an exact solution of the Navier–Stokes equations. Numerical integration of the integro-differential equations with different initial conditions shows that the equilibrium state of the flow is not unique after the first bifurcation point, but depends on the waveform of the initial disturbance or, equivalently, on ambient noise which cannot always be controlled in practical situations. Multiple equilibrium states are found to occur at the same value of the dynamic similarity parameters; this implies that any property transported by the fluid can at best be determined within a limit of uncertainty associated with nonuniqueness. A perturbation expansion with multiple time scales is used to show that the equations describing the evolution of monochromatic waves and slowly-varying wavepackets in classical weakly nonlinear theories are special limiting cases of the integro-differential equations near the onset of linear instability. The range of validity of the weakly nonlinear expansions is examined for mixed-convection flow in a heated vertical annulus. The results confirm that weakly nonlinear theories fail to give an adequate description of the physics of the flow even near the onset of linear instability. This is because these theories consider only the most unstable mode, and neglect the contribution from other eigenmodes which can have a large effect on the mean flow distortion. Without considering the leading-order effect of the mean-flow distortion, classical weakly nonlinear instability theories fail to account for proper energy exchanges. The numerical results of the integro-differential equations for the amplitude density function are compared with a direct numerical simulation of the Navier–Stokes equations using a Fourier–Chebyshev spectral method. Complete agreement is found between the two numerical solutions. The solution of the integro-differential equations is simpler than and requires only a small fraction of the computer time necessary for solving the Navier–Stokes equations by a spectral method. The current formulation presents an efficient algorithm to solve the Navier–Stokes equations.

1. INTRODUCTION

This study concerns nonlinear interactions among the travelling wave components of a continuous spectrum in fluid dynamics. Travelling waves frequently arise in fluid dynamics due to the growth of unstable disturbances. The critical wavenumber of the disturbance at the onset of instability may be predicted by a linearized analysis. The nonlinear growth of small-amplitude disturbances in the neighbourhood of the bifurcation point has commonly been studied using a perturbation method, as pioneered by Stuart [1] and Watson [2]. The weakly nonlinear theories of Stuart and Watson consider disturbances of travelling waves which are spatially periodic with wavelength $2\pi/k$, and study the generations of harmonics ($2k$, $3k$, etc.) of the fundamental mode and distortion of the mean flow due to nonlinear interactions. They are restricted to monochromatic waves. Linear instability analysis, however, indicates that a continuous finite band of wavenumbers can grow simultaneously. Stewartson and Stuart [3] extended the weakly nonlinear theory of monochromatic waves to incorporate a slow spatial modulation of the waves due to the interaction of a small continuous band of wavenumbers. They derived an equation to describe the spatio-temporal evolution of the envelope of the slowly varying wavepacket, which is similar to the equation for thermal convection derived previously by Newell and Whitehead [4] and Segel [5]. The weakly nonlinear theory of wavepackets is, however, valid only when the band of wavenumbers that can grow according to linear theory is so small that no energy can exchange among the wave components in the wavepacket. In this paper, an integral formalism is used to investigate the nonlinear interactions among waves of all possible wavenumbers.

Mixed convection flow in a heated vertical annulus is used as a model problem to study the nonlinear interactions among travelling waves. Recent work has

† Present address: Department of Mechanical Engineering, Indian Institute of Technology, Bombay, India.

NOMENCLATURE

A_m	amplitude density functions
C	constant determining average axial velocity of isothermal flow through annulus
d	distance between cylinders
E	disturbance kinetic energy
$E(k)$	kinetic energy of Fourier mode with wavenumber k
$\mathbf{e}_z$	unit vector in z direction
g	gravitational acceleration
G	axial pressure gradient
h	local heat transfer coefficient
k	axial wavenumber
k_f	final equilibrium wavenumber
$\bar{k}$	thermal conductivity of fluid
L	linear operators
N	number of waves or nonlinear operators
Nu	Nusselt number
Nu_z	local Nusselt number
p	pressure
Pr	Prandtl number
q_w	local heat flux at inner wall
Ra	Rayleigh number
Re	Reynolds number
r	radial coordinate
r_1	radius of inner cylinder (dimensional)
r_2	radius of outer cylinder (dimensional)
r_i	dimensionless radius of inner cylinder
r_o	dimensionless radius of outer cylinder
t	time
T	dimensional temperature
T_b	bulk temperature of fluid
T_o	upstream reference temperature
T_w	temperature of inner wall
u	radial velocity
$\hat{u}$	discrete Fourier transform of radial velocity
$\tilde{u}_m$	radial velocity predicted by linear stability theory
$\mathbf{u}$	$= (u, v, w)$, velocity vector
v	azimuthal velocity
$\tilde{v}_m$	azimuthal velocity predicted by linear stability theory
w	axial velocity
$\tilde{w}_m$	axial velocity predicted by linear stability theory
W	average axial velocity for isothermal flow through an annulus
W_0	fully developed axial velocity profile
y	normalized radial coordinate
z	axial coordinate.

Greek symbols

β	coefficient of thermal expansion
η	radius ratio of annulus
κ	thermal diffusivity of fluid
λ	wavelength of computational box
μ	axial temperature gradient
ν	kinematic viscosity of fluid
θ	dimensionless temperature
θ_0	fully developed temperature distribution
ρ	density of fluid
π	$= p + \frac{1}{2}\lvert\mathbf{u}\rvert^2$
ϕ	azimuthal angle
ω	$= \nabla \cdot \mathbf{u}$.

shown that parallel fully developed mixed convection flow in a heated vertical ducts is highly unstable due to thermally induced instabilities [6–13]. The presence of instabilities in nonisothermal flows in heated vertical ducts has been observed experimentally by Hanratty *et al.* [14], Kemeny and Somers [15] and Scheele and Hanratty [16]. These instabilities lead to significant increases in the heat transfer rates above those predicted by parallel-flow models. When the buoyancy forces aid the fluid motion, they observed that the initial transition resulted in a new equilibrium periodic flow pattern. However, when the buoyancy forces oppose the fluid motion, the transition to turbulence is abrupt. Thus, the observed bifurcation is supercritical when buoyancy forces aid the fluid motion, and may be subcritical when the buoyancy forces oppose the fluid motion. Similar instabilities have been observed by Maitra and Subba Raju [17] for flow in a heated vertical annulus.

The evolution of finite-amplitude disturbances in this flow situation was studied by Yao and Rogers [10] using weakly nonlinear instability theory. Their results indicate that the bifurcation is supercritical when buoyancy forces aid the fluid motion and are in agreement with the experiments of Maitra and Subba Raju. The time-dependent Navier–Stokes system was solved numerically by Yao and Ghosh Moulic [12] in the same flow situation using a Fourier–Chebyshev spectral method for different initial conditions. They found that the supercritical equilibrium state of the travelling waves bifurcating from fully-developed mixed convection flow is not unique, but depends on the waveform of the initial disturbance. In all cases, the equilibrium state consisted of a single dominant mode and its superharmonics. The range of equilibrium wavenumbers of this dominant mode was found to be narrower than the band of wavenumbers that can grow according to linear theory. Disturbances with wavenumbers outside this range but within the unstable region of linear theory were found to decay, their energy being transferred to a mode with wavenumber inside the narrow band. This result

is in agreement with the Eckhaus and Benjamin–Feir sideband instability [18]. It is worthy to point out that a *secondary* instability, like a sideband instability, is also a consequence of nonlinear energy transfer among different waves. The selection of the final equilibrium wavenumber is due to a nonlinear energy transfer process which is sensitive to initial conditions, and is not unique.

This nonuniqueness of the equilibrium state has been observed experimentally in Taylor–Couette [19, 21]. Snyder [19] showed that while the wavelength at the onset of instability was unique, Taylor vortex flows of different wavenumbers could be obtained at the same value of the Taylor number by varying the initial conditions in the experiments. He observed that there was a band of accessible wavenumbers narrower than the band that can grow according to linear theory. Burkhalter and Koschmeider [20] studied the variation of the wavelength of supercritical Taylor vortices. They found that Taylor vortices maintained the critical wavelength over a wide range of Taylor numbers if the Taylor number was varied quasi-steadily and end effects were taken into account. In a later article, Burkhalter and Koschmeider [21] reported results in which Taylor vortices were established through a sudden start of the inner cylinder. They found that a sudden start to a preset Taylor number gives the fluid a choice in the selection of the wavenumber. The nonlinear interactions among Taylor vortices with different wavenumbers was studied by Yao and Ghosh Moulic [13] using a weakly nonlinear theory formulated with a continuous spectrum. They represented the disturbance by a Fourier integral and derived an integro-differential equation for the evolution of the amplitude density of a continuous spectrum of waves. Solutions of this integro-differential equation indicated that the equilibrium state depended on the wavenumber and amplitude of the initial disturbance, as observed experimentally. They outlined selecting principles of equilibrium wavelengths from their numerical results. These principles can be used as a guide in selecting a possible range of equilibrium wavelengths in experiments. An important implication of the existence of non-unique equilibrium states is that the torque required to maintain the rotation of the cylinder at a constant speed cannot be determined uniquely after the first bifurcation point.

This principle of nonuniqueness has so far been observed experimentally only for closed systems such as Taylor and Bernard instabilities, and has been verified theoretically for the Taylor instability [13]. The numerical solution of Navier–Stokes equations demonstrated that the principle of nonuniqueness is also true for an open system, such as mixed-convection pipe flows [12]. Therefore, the principle of nonuniqueness is a generic property of all fluid flows. Consequently, any physical quantity transported by the fluid motion such as heat and salt can at best be determined within a limit of uncertainty associated with non-uniqueness after the first bifurcation point.

The analysis in Section 2 is developed to study the nonlinear evolution of a disturbance of arbitrary initial waveform. We consider a one-dimensional basic flow and study the stability of this flow to three-dimensional disturbances. The formulation can be extended to two-dimensional and three-dimensional basic states. The disturbance is represented by a continuous Fourier integral over all possible wavenumbers. The Fourier components of the disturbance quantities are then expanded in a series of linear stability eigenfunctions. The eigenfunction expansion reduces the Navier–Stokes equations to a system of coupled nonlinear integro-differential equations for the temporal evolution of the amplitude density function of a continuous spectrum of waves. No approximations are involved in this reduction. Thus, the integro-differential equations are equivalent to the Navier–Stokes equations. It is worth noting that although the integro-differential equations describe the temporal evolution of the amplitude density function in Fourier space, the integral formulation does allow the disturbance to have a general spatial variation in physical space and is not restricted to spatially periodic disturbances.

The eigenfunction expansion used in the current formulation implicitly assumes that the linear stability operator has an infinite set of discrete eigenvalues and a corresponding infinite set of eigenfunctions which form a complete set. There is no general proof of the completeness of the linear stability eigenfunctions. It has been shown that the Orr–Sommerfeld equation has a complete set of eigenfunctions for plane Couette flows [22] and plane Poiseuille flow [23]. DiPrima and Habetler [24] have proved a completeness theorem for a general class of non-self-adjoint eigenvalue problems in a finite bounded domain. Using this theorem, they have demonstrated that the Benard problem, the Taylor problem and the Orr–Sommerfeld equation for flow in a bounded domain have a complete set of eigenfunctions. These results, however, do not apply if the domain is infinite as in the case of the Blasius boundary-layer flow. Grosch and Salwen [25] showed that the Orr–Sommerfeld equation governing the stability of a shear flow in an unbounded domain which approaches a constant velocity in the far field has a continuous frequency spectrum. In this case, the disturbance quantities cannot be represented by a sum over only the discrete modes; the contribution from the continuous, or 'improper' eigenfunctions must be included [26]. There may also be cases where the linear stability operator has an infinite set of discrete eigenvalues, but all of the eigenvalues are not distinct. If the matrix corresponding to the discretized form of the linear stability operator is derogatory but non-defective, the eigenvectors are linearly independent [27]. If, however, the matrix is defective, some of the eigenvectors are linearly dependent. In the latter case, it is still possible to find a linearly independent set of

generalized eigenvectors [28]. In the present investigation, our numerical results have been verified by an independent computation using a Fourier–Chebyshev spectral method. This provides an indirect verification of the completeness of the linear stability eigenfunctions in this flow.

In Section 2.4, a perturbation expansion with multiple time scales is used to show that the equations describing the evolution of the amplitude of monochromatic waves and the envelope of slowly-varying wavepackets in classical weakly nonlinear theories are special limiting cases of this set of integro-differential equations in a parameter range close to the onset of linear instability. The reduction of the continuous formulation to the special limiting cases of monochromatic waves and wave-packets shows the limitations of the classical approaches. In particular, the Ginzburg–Landau equation describing the evolution of the envelope of a slowly-varying wavepacket is shown, at best, to be an approximation which is valid only locally in the neighbourhood of the onset of linear instability. This equation is known to have chaotic solutions [29–31]. The present investigation indicates that while this equation may have chaotic solutions, these solutions may not have physical relevance since the equation is not valid in a parameter range which is not near the linear neutral curve. Furthermore, solutions of the Ginzburg–Landau equation can only describe a slow spatial modulation of a periodic fluid motion with a single dominant wavenumber, and is incapable of describing chaotic fluid motion with a general spatial variation. Solutions of the integro-differential equations in the current formulation, on the other hand, are valid for all parameters, include full spectra and can describe chaotic fluid motions properly. The current formulation thus provides the proper framework for the study of spatio-temporal chaos.

The integro-differential equations have been solved numerically with different initial conditions for supercritical Rayleigh numbers. In all cases, the final equilibrium state was found to be a monochromatic travelling wave with a dominant fundamental wavenumber k_f and its superharmonics, and an associated mean flow distortion with the values of the selected parameters. Nonlinear interactions were found to excite a number of eigenmodes for the fundamental wave ($k = k_f$) and its harmonics, and the mean flow distortion ($k = 0$). The equilibrium wave-speeds of all the eigenmodes were found to be the same. Thus, the harmonics of the fundamental wave k_f are phase-locked at equilibrium. The fundamental wavenumber k_f in the final equilibrium state was found to depend on the initial conditions. Thus, the equilibrium state of the flow is not unique. Multiple stable equilibrium states are found to exist at the same value of the dynamic similarity parameters. The results imply that the selection of this wavenumber k_f is a natural consequence of a nonlinear energy transfer process and depends on the initial conditions. The current formulation with a continuous spectrum allows us to study the nonlinear evolution of the disturbance from an arbitrary initial waveform as well as the proper selection of the equilibrium wavenumber.

The solution of the integro-differential equations indicates that the equilibrium amplitudes of some of the eigenmodes for the mean distortion are larger than the amplitude of the most unstable eigenmode of the fundamental wave even at Rayleigh numbers less than 1% above the critical value. This implies that classical weakly nonlinear theories which assume *a priori* that the energy associated with the mean flow distortion induced by the fundamental wave is an order of magnitude smaller than the energy of the fundamental wave, are not valid, even in a parameter range very close to the onset of linear instability where the weakly nonlinear analysis may be expected to be valid. The reason for the failure of the classical theories is that these theories consider only the most unstable eigenmode. Our computation indicates that the contribution from the other eigenmodes has a large effect on the mean flow distortion even near the onset of instability. Thus, it is inadequate to consider only the most unstable eigenmode, although this assumption leads to a considerable simplification in the analysis.

The solutions also show that there are two types of nonlinear interaction between waves. One is direct interaction, if they satisfy the resonance condition, which has been pointed out by Landau and is analysed in detail in Section 2.4. The other is *indirect* interaction in which the waves interact simultaneously with the mean flow ($k = 0$). The resonance condition for indirect interaction is always satisfied and the indirect interaction constantly exists, but has been overlooked in classical theories.

The results of the numerical integration of the integro-differential equations are compared with the results of a direct numerical simulation of the time-dependent Navier–Stokes equations using a Fourier–Chebyshev spectral method [12]. Complete agreement is found between the two numerical solutions, as expected, since they are both exact solutions of the Navier–Stokes equations. The eigenfunction expansion used in the current formulation requires only one amplitude density function for the all dependent variables, such as the velocity components and temperature. Thus, the three momentum equations and the energy equation is replaced by a single equation for the amplitude density function. Consequently, the number of operations involved in the numerical solution of the integro-differential equations is much less than that involved in a Fourier–Chebyshev spectral method. The required CPU time for the solution of the integro-differential equations of the current two-dimensional problem is only 25% of that required for the direct numerical simulation. Our formulation presents an efficient numerical method for solving the time-dependent Navier–Stokes equations with significant savings in computer time. The two computations were done on a CRAY C-90 supercomputer,

and both computer codes were fully optimized to take advantage of the vector facilities on the CRAY. Thus, the relative CPU time for the two computations is a true indication of the computational efficiency of the current formulation.

2. ANALYSIS

In this section, we develop a general formulation to study nonlinear interactions among travelling waves in cylindrical coordinates. We consider a steady one-dimensional basic flow and study the stability of this flow to three-dimensional disturbances of arbitrary waveform. The formulation can be generalized to three-dimensional basic-states. The disturbance is represented by a Fourier integral, and a system of equations describing the nonlinear wave interactions among the Fourier components is derived in Section 2.1. The linear stability of the basic flow is analysed in Section 2.2. The solution of the nonlinear disturbance equations is considered in Section 2.3 by expanding the Fourier components in a series, using the eigenfunctions of linear stability theory as the basis functions. The eigenfunction expansion reduces the Navier–Stokes system to a set of integro-differential equations for the amplitude density function of a continuous spectrum. No approximations are involved in this reduction. Thus, the integro-differential equations are equivalent to the Navier–Stokes equations. A perturbation expansion based on the method of multiple scales is used in Section 2.4 to show that the equations describing the evolution of the amplitude of monochromatic waves and the envelope of slowly-varying wavepackets in classical weakly nonlinear theories are special limiting cases of this set of integro-differential equations. In order to demonstrate this, we follow the classical approach and solve the Navier–Stokes equations directly in Section 2.4.2 using a perturbation method before doing the eigenfunction expansion. The resulting solution is compared with the perturbation solution of the integro-differential equations resulting from the eigenfunction expansion presented in Section 2.4.1, in order to show the equivalence between the two approaches. In Section 2.4.3, we consider the important special cases of monochromatic waves and slowly-varying wavepackets.

Mixed convection flow in a heated annulus is used as a model problem to develop the formulation. We consider the flow in a vertical annulus, driven by an external pressure gradient, as illustrated in Fig. 1. A constant vertical temperature gradient is maintained at the inner cylinder, and the outer cylinder is insulated. The temperature of the inner wall increases linearly with the axial coordinate from an upstream reference temperature, T_0, as $T_w = T_0 + \mu\bar{z}$, where μ is the constant vertical temperature gradient and $\bar{z}$ is the (dimensional) axial coordinate. In the limiting case of fully developed flow, this simulates a uniform heat flux thermal boundary condition on the inner cylinder. The equations describing the flow are the continuity, momentum and energy equations. Using the Boussinesq approximation, these equations may be written in dimensionless form as

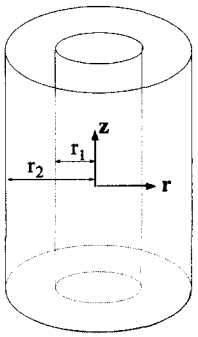

Fig. 1. Geometry and coordinates.

$$\nabla\cdot\mathbf{u} = 0$$

$$\frac{\partial\mathbf{u}}{\partial t} + \mathbf{u}\cdot\nabla\mathbf{u} = \frac{C}{Re}\mathbf{e}_z - \nabla p + \frac{1}{Re}\nabla^2\mathbf{u} - \frac{Ra}{Re}\theta\mathbf{e}_z \quad (1)$$

$$\frac{\partial\theta}{\partial t} + \mathbf{u}\cdot\nabla\theta = \frac{1}{RePr}\nabla^2\theta + \frac{w}{RePr}$$

where $\mathbf{e}_z$ is the unit vector along the z direction, $\mathbf{u} = (u, v, w)$ are the velocity components in the r, ϕ and z directions respectively, p is the pressure, θ is the temperature and t is the time. All lengths have been scaled by the distance between the cylinders, $d = r_2 - r_1$, where r_1 is the radius of the inner cylinder and r_2 is the radius of the outer cylinder. Our choice of the velocity scale is based on the applied axial pressure gradient, G. The average axial velocity for isothermal flow through an annulus is given by $W_{ave} = Gd^2/(\rho\nu C)$, where $C = 8\ (1-\eta)/[(1+\eta^2)/((1-\eta)+(1+\eta)/\ln\eta)]$, $\eta = r_1/r_2$ is the radius ratio of the annulus, ρ is the density of the fluid and ν is the kinematic viscosity. This provides a natural velocity scale for this problem. A non-dimensional pressure is defined by $p = (\bar{p} + Gdz)/\rho W_{ave}^2$, where $\bar{p}$ is the (dimensional) pressure fluctuation. The time is scaled by d/W_{ave}. The dimensionless temperature is defined by $\theta = (T_w - T)/\mu dRePr$. The parameters in the problem are the Reynolds number $Re = W_{ave}d/\nu$, the Prandtl number $Pr = \nu/\kappa$, and the Rayleigh number $Ra = \mu\beta g d^4/(\nu\kappa)$. Here, β is the coefficient of thermal expansion of the fluid, κ is the thermal diffusivity and g is the gravitational acceleration. The boundary conditions are

$$u = v = w = \theta = 0 \quad \text{when } r = r_i \quad (2)$$

$$\text{and} \quad u = v = w = \frac{\partial\theta}{\partial r} = 0 \quad \text{when } r = r_0$$

where $r_i = r_1/d$, and $r_0 = r_2/d$.

2.1. *The disturbance equations in Fourier space*

The equations (1) admit a steady parallel-flow solution $u = v = 0$, $w = W_0(r)$, $\theta = \theta_0(r)$. The stability of this parallel flow is studied by superposing a dis-

turbance on the basic flow, and writing the disturbed velocity and thermal fields as

$$(u, v, w, \theta) = (u', v', W_0(r) + w', \theta_0(r) + \theta') \quad (3)$$

where the primes denote disturbance quantities. It is worthwhile to point out that the magnitude of the disturbances do not have to be small. Substitution of (3) into (1) leads to a system of equations for the disturbance quantities. Following Yao and Ghosh Moulic [13], the disturbance quantities are expressed in their most general form as Fourier integrals over all possible axial wavenumbers. The Fourier transforms of the disturbance variables are then expressed as a Fourier series over the integer azimuthal wavenumbers. Thus, the axial component of the disturbance velocity is written as

$$w'(r, \phi, z, t) = \sum_{n=-\infty}^{\infty} \int_{-\infty}^{\infty} \hat{w}(k, n, r, t)\, e^{ikz + in\phi}\, dk. \quad (4)$$

Similar expressions may be written for the other disturbance quantities. The disturbance equations in Fourier space may be expressed as

$$D\hat{u}(k, n, r, t) + \frac{\hat{u}(k, n, r, t)}{r} + \frac{in\hat{v}(k, n, r, t)}{r} + ik\hat{w}(k, n, r, t) = 0$$

$$\frac{\partial \hat{U}_j}{\partial t}(k, n, r, t) + L_j(k, n, \hat{U}(k, n, r, t), \hat{p}(k, n, r, t)) = \hat{N}_j(k, n, r, t) \quad (5)$$

where

$$\hat{\mathbf{U}}(k, n, r, t) = (\hat{\mathbf{u}}(k, n, r, t), \hat{\theta}(k, n, r, t)) = (\hat{u}(k, n, r, t), \hat{v}(k, n, r, t), \hat{w}(k, n, r, t), \hat{\theta}(k, n, r, t))$$

the linear operators L_j are given by

$$L_1(k, n, \hat{\mathbf{U}}(k, n, r, t), \hat{P}(k, n, r, t)) = -\frac{1}{Re}\left[L\hat{u}(k, n, r, t) - \frac{\hat{u}(k, n, r, t)}{r^2} - \frac{2in\hat{v}(k, n, r, t)}{r^2}\right] + ikW_0(r)\hat{u}(k, n, r, t) + D\hat{P}(k, n, r, t)$$

$$L_2(k, n, \hat{\mathbf{U}}(k, n, r, t), \hat{P}(k, n, r, t)) = -\frac{1}{Re}\left[L\hat{v}(k, n, r, t) - \frac{\hat{v}(k, n, r, t)}{r^2} + \frac{2in\hat{u}(k, n, r, t)}{r^2}\right] + ikW_0(r)\hat{v}(k, n, r, t) + \frac{in\hat{P}(k, n, r, t)}{r}$$

$$L_3(k, n, \mathbf{U}(k, n, r, t), \hat{P}(k, n, r, t)) = -\frac{1}{Re}L\hat{w}(k, n, r, t) + \frac{Ra}{Re}\hat{\theta}(k, n, r, t) + ikW_0(r)\hat{w}(k, n, r, t) + D[W_0(r)\hat{u}(k, n, r, t)] + ik\hat{P}(k, n, r, t)$$

$$L_4(k, n, \hat{\mathbf{U}}(k, n, r, t), \hat{P}(k, n, r, t)) = -\frac{1}{RePr}L\hat{\theta}(k, n, r, t) - \frac{\hat{w}(k, n, r, t)}{RePr} + ikW_0(r)\hat{\theta}(k, n, r, t) + D[\theta_0(r)\hat{u}(k, n, r, t)] \quad (6)$$

$L \equiv D^2 + (1/r)D - (n^2/r^2) - k^2$, $D \equiv (d/dr)$ is the operator denoting differentiation with respect to the radial coordinate, and $\hat{N}_j(k, n, r, t)$ represents the nonlinear convection terms in Fourier space defined by

$$\hat{N}_j(k, n, r, t) = \begin{cases} -\dfrac{1}{(2\pi)^2}\displaystyle\int_{-\infty}^{\infty}\int_0^{2\pi} (\mathbf{u}' \cdot \nabla u_j') e^{-i(kz + n\phi)}\, d\phi\, dz, \\ \qquad\qquad j = 1, 2, 3 \\ -\dfrac{1}{(2\pi)^2}\displaystyle\int_{-\infty}^{\infty}\int_0^{2\pi} (\mathbf{u}' \cdot \nabla \theta') e^{-i(kz + n\phi)}\, d\phi\, dz, \\ \qquad\qquad j = 4. \end{cases} \quad (7)$$

We have used the index notation $\hat{U}_1 = \hat{u}$, $\hat{U}_2 = \hat{v}$, $\hat{U}_3 = \hat{w}$ and $\hat{U}_4 = \hat{\theta}$ in order to write the disturbance equations (5) in compact form. Equations (7) and (8) may be expressed in convolution form as

$$\hat{N}_j(k, n, r, t) = -\sum_{n_1=-\infty}^{\infty} \int_{-\infty}^{\infty} M_j(k, n, \hat{\mathbf{U}}(k_1, n_1, r, t), \hat{\mathbf{U}}(k - k_1, n - n_1, r, t))\, dk_1 \quad (8)$$

where N_j denote nonlinear operators given by

$$M_1(k, n, \hat{\mathbf{U}}(k_1, n_1, r, t), \hat{\mathbf{U}}(k_2, n_2, r, t)) = D[\hat{u}(k_1, n_1, r, t)\hat{u}(k_2, n_2, r, t)] + \frac{\hat{u}(k_1, n_1, r, t)\hat{u}(k_2, n_2, r, t)}{r} - \frac{\hat{v}(k_1, n_1, r, t)\hat{v}(k_2, n_2, r, t)}{r} + \frac{2in_1\hat{u}(k_1, n_1, r, t)\hat{v}(k_2, n_2, r, t)}{r} + 2ik_1\hat{u}(k_1, n_1, r, t)\hat{w}(k_2, n_2, r, t)$$

$$M_2(k, n, \hat{\mathbf{U}}(k_1, n_1, r, t), \hat{\mathbf{U}}(k_2, n_2, r, t)) = D[\hat{u}(k_1, n_1, r, t)\hat{v}(k_2, n_2, r, t)] + \frac{2\hat{u}(k_1, n_1, r, t)\hat{v}(k_2, n_2, r, t)}{r} + \frac{2in_1\hat{v}(k_1, n_1, r, t)\hat{v}(k_2, n_2, r, t)}{r} + 2ik_1\hat{w}(k_1, n_1, r, t)\hat{v}(k_2, n_2, r, t)$$

$$M_3(k, n, \hat{\mathbf{U}}(k_1, n_1, r, t), \hat{\mathbf{U}}(k_2, n_2, r, t)) = D[\hat{u}(k_1, n_1, r, t)\hat{w}(k_2, n_2, r, t)] + \frac{\hat{u}(k_1, n_1, r, t)\hat{w}(k_2, n_2, r, t)}{r}$$

$$+\frac{2in_1\hat{v}(k_1,n_1,r,t)\hat{w}(k_2,n_2,r,t)}{r}$$

$$+2ik_1\hat{w}(k_1,n_1,r,t)\hat{w}(k_2,n_2,r,t)$$

$$M_4(k,n,\hat{\mathbf{U}}(k_1,n_1,r,t),\hat{\mathbf{U}}(k_2,n_2,r,t))$$

$$=D[\hat{u}(k_1,n_1,r,t)\hat{\theta}(k_2,n_2,r,t)]$$

$$+\frac{\hat{u}(k_1,n_1,r,t)\hat{\theta}(k_2,n_2,r,t)}{r}$$

$$+\frac{2in_1\hat{v}(k_1,n_1,r,t)\hat{\theta}(k_2,n_2,r,t)}{r}$$

$$+2ik_1\hat{w}(k_1,n_1,r,t)\hat{\theta}(k_2,n_2,r,t). \quad (9)$$

The convolution integrals in equation (5) represent the nonlinear terms exactly. Equations (5) have to be solved subject to the boundary conditions

$$\hat{u}(k,n,r,t)=\hat{v}(k,n,r,t)=\hat{w}(k,n,r,t)=\hat{\theta}(k,n,r,t)=0 \quad \text{at } r=r_i \quad (10)$$

and

$$\hat{u}(k,n,r,t)=\hat{v}(k,n,r,t)=\hat{w}(k,n,r,t)=D\hat{\theta}(k,n,r,t)=0 \quad \text{at } r=r_o.$$

It is worth noting that while the spectrum of the disturbance quantities expressed by equation (4) is continuous in the axial wavenumber k, it is discrete in the azimuthal wavenumber n, due to the requirement of periodicity in the azimuthal direction.

2.2. *Linear stability*

The linear stability of the basic flow is studied by assuming the disturbance to be infinitesimally small, neglecting the convolution integrals which represent products of infinitesimal quantities, and expressing the Fourier components of the disturbance quantities in separable form as

$$\hat{\mathbf{U}}(k,n,r,t)=\tilde{\mathbf{U}}(k,n,r)e^{-i\omega(k,n)t} \quad (11)$$

where $\omega(k,n)=\omega^R(k,n)+i\omega^I(k,n)$ is the complex frequency for the wavenumbers (k,n) and the superscripts "R" and "I" denote the real and imaginary parts of the complex frequency. The linearized disturbance equations may be written in terms of the operators L_j as

$$D\tilde{u}(k,n,r)+\frac{\tilde{u}(k,n,r)}{r}+\frac{in\tilde{v}(k,n,r)}{r}+ik\tilde{w}(k,n,r)=0$$

$$L_j(k,n,\tilde{\mathbf{U}}(k,n,r),\tilde{p}(k,n,r))=i\omega(k,n)\tilde{U}_j(k,n,r) \quad (12)$$

where $\tilde{\mathbf{U}}(k,n,r)$ is the vector of eigenfunctions $(\tilde{u}(k,n,r),\ \tilde{v}(k,n,r),\ \tilde{w}(k,n,r),\ \tilde{\theta}(k,n,r))$. The associated boundary conditions are the same as those given by equations (10). Equations (12) with the appropriate boundary conditions form an eigenvalue problem for the complex frequency $\omega(k,n)$, with the disturbance being linearly unstable for $\omega^I(k,n)>0$.

2.3. *Nonlinear formulation*

In this section, the disturbance equations (5) are solved by an eigenfunction expansion. The solution of equations (5) is expressed as

$$\hat{\mathbf{U}}(k,n,r,t)=\sum_{m=1}^{\infty}A_m(k,n,t)\tilde{\mathbf{U}}_m(k,n,r) \quad (13)$$

where $\tilde{\mathbf{U}}_m(k,n,r)$ is the eigenfunction of the linearized equations (12) corresponding to the mth eigenvalue $\omega_m(k,n)$ and $A_m(k,n,t)$ is a time-dependent amplitude density function. The eigenvalues, ω_m, of the linear-instability operator are ordered so that $\omega_1^I\geqslant\omega_2^I\geqslant\omega_3^I\geqslant\ldots$. Thus, the first eigenvalue represents the least stable or the most unstable mode. The eigenfunctions are normalized so that

$$\int_{r_i}^{r_o}[|\tilde{u}_m|^2+|\tilde{v}_m|^2+|\tilde{w}_m|^2]r\,dr=1.$$

The amplitude density function is determined by substituting the eigenfunction expansion (13) into the disturbance equations (5) and using the orthogonality relation between the eigenfunctions $\tilde{\mathbf{U}}(k,n,r)$ of the linearized equations (12) and the corresponding adjoint eigenfunctions $\mathbf{U}^\dagger(k,n,r)=(u^\dagger,v^\dagger,w^\dagger,\theta^\dagger)$. We define an inner product between the vectors $\tilde{\mathbf{U}}$ and $\mathbf{U}^\dagger$ by $\langle\mathbf{U}^\dagger,\tilde{\mathbf{U}}\rangle=\langle u^\dagger,\tilde{u}\rangle+\langle v^\dagger,\tilde{v}\rangle+\langle w^\dagger,\tilde{w}\rangle+\langle\theta^\dagger,\tilde{\theta}\rangle$, where the inner product between two scalar functions $f(r)$ and $g(r)$ is defined as

$$\langle f,g\rangle=\int_{r_i}^{r_o}f^*g\,dr$$

and the asterisk denotes complex conjugates. If the adjoint eigenfunctions are normalized so that

$$\langle\mathbf{U}_m^\dagger(k,n,r),\tilde{\mathbf{U}}_j(k,n,r)\rangle=\delta_{j,m} \quad (14)$$

where $\delta_{j,m}$ is the Kronecker delta, taking the inner product of the r-momentum equation with $u_m^\dagger$, the ϕ-momentum equation with $v_m^\dagger$, the z-momentum equation with $w_m^\dagger(k,n,r)$ and the energy equation with $\theta_m^\dagger(k,n,r)$ and adding yields, on using the orthogonality property (14) of the eigenfunctions and the continuity equation, the following system of coupled nonlinear integro-differential equations for the amplitude density functions:

$$\frac{dA_m}{dt}+i\omega_mA_m=\langle\mathbf{U}_m^\dagger,\hat{\mathbf{N}}\rangle \quad (15)$$

where $\hat{\mathbf{N}}=(\hat{N}_1,\hat{N}_2,\hat{N}_3,\hat{N}_4)$. This is equivalent to the Fredholm alternative theory. Using equation (8), equation (15) may be expressed as

$$\frac{dA_m}{dt}+i\omega_mA_m=\sum_{m_1=1}^{\infty}\sum_{m_2=1}^{\infty}\sum_{n_1=-\infty}^{\infty}I(k,n,m,m_1,m_2,n_1,t) \quad (16)$$

where

$$I = \int_{-\infty}^{\infty} b(k_1, k-k_1, n_1, n-n_1, m_1, m_2, m) \cdot A_{m_1}(k_1, n_1, t)\, A_{m_2}(k-k_1, n-n_1, t)\, \mathrm{d}k_1$$

and the interaction coefficients

$$b = \langle \mathbf{U}_m^{\dagger}(k, n, r), \mathbf{M}(k, n, \tilde{U}_{m_1}(k_1, n_1, r), \tilde{U}_{m_2}(k-k_1, n-n_1, r)) \rangle$$

depend on the eigenfunctions of the linearized equations (12) and the corresponding adjoint eigenfunctions, and are independent of time.

It is instructive to write the complex amplitude density function in polar form as $A_m(k, n, t) = R_m(k, n, t)\, \mathrm{e}^{i\beta_m(k,n,t)}$, where $R_m = |A_m| = \sqrt{(A_m^{\mathrm{R}^2} + A_m^{\mathrm{I}^2})}$ is the magnitude and $\beta_m = \tan^{-1}(A_m^{\mathrm{I}}/A_m^{\mathrm{R}})$ is the phase angle. The complex amplitude equation (16) may be expressed in polar form as

$$\frac{\mathrm{d}R_m}{\mathrm{d}t} = \omega_m^{\mathrm{I}} R_m + I_m^{\mathrm{r}} \tag{17}$$

$$\frac{\mathrm{d}\beta_m}{\mathrm{d}t} = -\omega_m^{\mathrm{R}} + I_m^{\beta} \tag{18}$$

where

$$I_m^{\mathrm{r}} = \sum_{m_1=1}^{\infty} \sum_{m_2=1}^{\infty} \sum_{n_1=-\infty}^{\infty} \int_{-\infty}^{\infty} \{b^{\mathrm{I}} \cos\psi - b^{\mathrm{R}} \sin\psi\} \cdot R_{m_1}(k_1, n_1, t) R_{m_2}(k-k_1, n-n_1, t)\, \mathrm{d}k_1$$

$$I_m^{\beta} = \sum_{m_1=1}^{\infty} \sum_{m_2=1}^{\infty} \sum_{n_1=-\infty}^{\infty} \int_{-\infty}^{\infty} \{b^{\mathrm{R}} \cos\psi + b^{\mathrm{I}} \sin\psi\} \cdot \frac{R_{m_1}(k_1, n_1, t) R_{m_2}(k-k_1, n-n_1, t)}{R_m(k, n, t)}\, \mathrm{d}k_1$$

$$\psi(k, n, m, k_1, n_1, m_1, m_2, t) = \beta_{m_1}(k_1, n_1, t) + \beta_{m_2}(k-k_1, n-n_1, t) - \beta_m(k, n, t),$$

and b^{R} and b^{I} are the real and imaginary parts of b, respectively. The first term on the right-hand side of equation (17) is the amplification or decay rate predicted by linear stability theory and represents energy transfer due to linear convection and viscous effects. The convolution integrals represent energy transfer among the wave components due to nonlinear wave interactions. The first term on the right-hand side of equation (18) is the frequency predicted by linear theory. The second term in equation (18) represents a modification in the frequency due to nonlinear effects. It is worth noting that the fixed points of equation (17), obtained by setting $\mathrm{d}R_m/\mathrm{d}t = 0$, represent an equilibrium time-periodic travelling wave solution with amplitudes which are steady. Equation (17) indicates that this equilibrium solution is possible only if the relative phase angle ψ is independent of time, that is, if $\mathrm{d}\psi/\mathrm{d}t = 0$. Since the frequencies of the eigenmodes for a given wavenumber predicted by linear theory are not necessarily equal, phase-locking can occur only if nonlinear effects synchronize the waves so that all the eigenmodes travel with the same phase speed.

The eigenfunction expansion (13) has reduced the three momentum equations and the energy equation to the system of integro-differential equations for the amplitude density functions (16) without any approximations. Thus, the solution of equations (16) represents a solution of the Navier–Stokes equations. The linear terms on the left-hand side of (5), which represent the convection of the disturbance waves by the mean flow, the distortion by the mean-flow stresses and by the buoyant-body forces, and the diffusions of momentum and energy, are reduced to a single term in (16), which describes the growth or decay of the wave in the generalized coordinates of the eigenfunctions. This is a drastic simplification of the governing equations due to the fact that the eigenfunctions of the linear stability analysis form the *fundamental solutions* of the problem. These fundamental solutions may share many similarities for certain classes of problems, but differ in detail. It is unlikely that a universal solution exists for all fluid flows. The growth rate of the disturbances and the mean flow can be substantially altered by the nonlinear energy transfer among them. The nonlinear energy transfers are represented by the convolution integrals on the right-hand side of (16). In Section 2.4, we will show that the convolution integrals represent resonant triads, quartets, and so forth. The significance of the nonlinear wave interactions decreases as the number of involved waves increases.

Equations (16) may be solved numerically. It is worth pointing out that one of the major difficulties in the numerical solution of the incompressible Navier–Stokes system is the simultaneous enforcement of the no-slip boundary conditions and the incompressibility constraint [32]. Since the vector of basis functions used in the expansion (13) are solutions of the linearized Navier–Stokes equations, they individually satisfy the incompressibility constraint as well as the boundary conditions. Therefore, the expansion (13) automatically satisfies the boundary conditions and the continuity equation. Thus, the numerical solution of the system of equations (16) is much simpler than the numerical solution of the Navier–Stokes equations. It may also be noted that straightforward evaluation of the convolution product representing the nonlinear terms in equation (16) is inefficient if the number of terms in the truncated eigenfunction expansion used in the numerical solution is large. However, pseudospectral evaluation of the convolution product can make the numerical solution of the equations (15) a viable efficient alternative to the numerical solution of the Navier–Stokes equations.

2.4. *Limiting cases*

In the following, we will demonstrate that weakly nonlinear flow instability or wave interaction is a limiting case of the nonlinear formulation presented

above in a parameter range close to the onset of linear instability.

2.4.1. *Expansion and perturbation.* The weakly nonlinear development of the disturbances may be studied by expanding the Fourier amplitudes in a perturbation series. The maximum amplification rate predicted by linear instability theory is used as the expansion parameter ε [13]. The amplification rate predicted by linear theory for the mth eigenmode of the wave with axial wavenumber k and azimuthal wavenumber n may be expressed in terms of ε as $\omega_m^{\mathrm{I}}(k,n) = \varepsilon a_m(k,n)$. This makes $a_m(k,n)$ a constant of order one. It may be noted that the ordering used in the perturbation expansion in Section 2.4 differs from the ordering in the weakly nonlinear theory of monochromatic waves [1]. The wave components of a continuous spectrum may exchange energy due to quadratic nonlinear interactions among resonant triads of wavenumbers. Nonlinear interactions among resonant triads may play an important role in the laminar–turbulent transition process in some shear flows [33, 34]. Such nonlinear interactions among resonant triads are absent in monochromatic waves and slowly varying wavepackets. The present ordering allows the possibility of nonlinear interactions among resonant triads, and consequently differs from the usual ordering of classical weakly nonlinear theories of monochromatic waves. In the special limiting cases of monochromatic waves and slowly-varying wavepackets, the final form of the amplitude equations obtained from the current formulation is the same as those in classical weakly nonlinear theories.

It is convenient to write the coefficients in the eigenfunction expansion (13) as

$$A_m(k,n,t) = \tilde{A}_m(k,n,t)\,\mathrm{e}^{-i\omega_m^{\mathrm{R}}(k,n)t} \tag{19}$$

where ω_m^{R} is the (real) frequency predicted by linear theory, so that equation (16) takes the form

$$\frac{\mathrm{d}\tilde{A}_m}{\mathrm{d}t} = \varepsilon a_m \tilde{A}_m + \sum_{m_1=1}^{\infty}\sum_{m_2=1}^{\infty}\sum_{n_1=-\infty}^{\infty}\tilde{I}(k,n,m,m_1,m_2,n_1,t) \tag{20}$$

where

$$\tilde{I} = \int_{-\infty}^{\infty} b\tilde{A}_{m_1}(k_1,n_1,t)\tilde{A}_{m_2}(k-k_1,n-n_1,t)\,\mathrm{e}^{i\Omega_{3w}t}\,\mathrm{d}k_1$$

and

$$\Omega_{3w} = \omega_m^{\mathrm{R}}(k,n) - \omega_{m_1}^{\mathrm{R}}(k_1,n_1) - \omega_{m_2}^{\mathrm{R}}(k-k_1,n-n_1).$$

The amplitude density function $\tilde{A}_m$ is further expanded in a perturbation series as

$$\tilde{A}_m(k,n,t) = \varepsilon A_{m,1}(k,n,t,T_1,T_2) + \varepsilon^2 A_{m,2}(k,n,t,T_1,T_2) + \varepsilon^3 A_{m,3}(k,n,t,T_1,T_2) + \ldots \tag{21}$$

where $T_1 = \varepsilon t$ and $T_2 = \varepsilon^2 t$ are slow time scales. Substitution of the expansion (21) into equation (20) results in a set of equations at different orders on equating coefficients of like powers of ε. The leading order equation is

$$\frac{\partial A_{m,1}}{\partial t}(k,n,t,T_1,T_2) = 0. \tag{22}$$

Equation (22) indicates that the leading order amplitude density function is independent of the fast time scale t. The equation at second order is

$$\frac{\partial A_{m,2}}{\partial t}(k,n,t,T_1,T_2) = -\left[\frac{\partial A_{m,1}}{\partial T_1}(k,n,T_1,T_2) - a_m(k,n)A_{m,1}(k,n,T_1,T_2)\right] + \sum_{m_1,m_2}\sum_{n_1}\tilde{I}_1(k,n,m,m_1,m_2,n_1,t,T_1,T_2) \tag{23}$$

where

$$\tilde{I}_1 = \int_{-\infty}^{\infty} bA_{m_1,1}(k_1,n_1,T_1,T_2)\cdot A_{m_2,1}(k-k_1,n-n_1,T_1,T_2)\,\mathrm{e}^{i\Omega_{3w}t}\,\mathrm{d}k_1.$$

The summations over m_1 and m_2 range from 1 to ∞, while the summation over n_1 ranges from $-\infty$ to ∞. The integrals on the right-hand side of equation (23) depends on the fast time scale t, as well as the slow time scales T_1 and T_2. The integrands oscillate on the fast time scale with a frequency Ω_{3w}. It is worthwhile to note that the dispersion relation allows a three-wave resonance if $\Omega_{3w} = 0$. When this condition is satisfied, the integrands do not depend on the fast time scale. Thus, the forcing function on the right-hand side of equation (23) may be split into two parts: (a) a "steady part", which is independent of the fast time scale t, and (b) an oscillatory part which depends on the fast time scale. The steady part of the forcing function will invoke a resonant response which grows linearly in t. Elimination of the secular terms yields the following equation for the evolution of the leading order amplitude density function on the T_1 time scale:

$$\frac{\partial A_{m,1}}{\partial T_1} = a_m A_{m,1} + \sum_{m_1,m_2}\sum_{n_1}\tilde{I}_1^{\mathrm{S}}(k,n,m,m_1,m_2,n_1,T_1,T_2) \tag{24}$$

where $\tilde{I}_1^{\mathrm{S}}$ is the "steady part" of the integral $\tilde{I}_1$. The steady part of the integral is determined by contribution from the neighborhood of points satisfying the three-wave resonance condition $\Omega_{3w} = 0$. If there are N disjoint regions $k_j^{\mathrm{L}} \leqslant k_1 \leqslant k_j^{\mathrm{U}}$, $j = 1,2,\ldots,N$ over which the three-wave resonance condition is satisfied, the steady part of the integral is given by a summation of integrals over these N regions:

$$\tilde{I}_1^{\mathrm{S}} = \sum_{j=1}^{N}\int_{k_j^{\mathrm{L}}}^{k_j^{\mathrm{U}}} bA_{m_1,1}(k_1,n_1,T_1,T_2)\cdot A_{m_2,1}(k-k_1,n-n_1,T_1,T_2)\,\mathrm{d}k_1$$

or compactly

$$\tilde{I}_1^S = \int_{-\infty}^{\infty} b^S A_{m_1,1}(k_1, n_1, T_1, T_2) \cdot A_{m_2,1}(k-k_1, n-n_1, T_1, T_2)\, dk_1,$$

where the coefficient

$$b^S = \begin{cases} b, & k_j^L \leqslant k_1 \leqslant k_j^U, \quad j = 1, \ldots N \\ 0, & \text{otherwise.} \end{cases}$$

Triads of wavenumbers (k_1, n_1), $(k-k_1, n-n_1)$ and (k, n), which satisfy this condition, called resonant triads, exchange a significant amount of energy on the T_1 time scale. Substitution of equation (24) into the right-hand side of equation (23) leads to

$$\frac{\partial A_{m,2}}{\partial t} = \sum_{m_1, m_2} \sum_{n_1} \tilde{I}_1^T(k, n, m, m_1, m_2, n_1, t, T_1, T_2) \tag{25}$$

where

$$\tilde{I}_1^T = \int_{-\infty}^{\infty} b^T A_{m_1,1}(k_1, n_1, T_1, T_2) \cdot A_{m_2,1}(k-k_1, n-n_1, T_1, T_2)\, e^{i\Omega_{3w} t}\, dk_1$$

is the time-dependent part of the forcing function and $b^T = b - b^S$. Integration of equation (25) with respect to the fast time scale yields the second order amplitude density function

$$A_{m,2} = \sum_{m_1, m_2} \sum_{n_1} \int_{-\infty}^{\infty} b^T A_{m_1,1}(k_1, n_1, T_1, T_2) \cdot A_{m_2,1}(k-k_1, n-n_1, T_1, T_2) \frac{e^{i\Omega_{3w} t}}{i\Omega_{3w}} dk_1. \tag{26}$$

The amplitude density function at third order is described by the equation

$$\begin{aligned} \frac{\partial A_{m,3}}{\partial t} = & -\frac{\partial A_{m,1}}{\partial T_2} - \left[\frac{\partial A_{m,2}}{\partial T_1} - a_m(k,n) A_{m,2}\right] \\ & + \sum_{m_1, m_2} \sum_{n_1} \int_{-\infty}^{\infty} b[A_{m_1,1}(k_1, n_1, T_1, T_2) \cdot A_{m_2,2}(k-k_1, n-n_1, t, T_1, T_2) \\ & + A_{m_1,2}(k_1, n_1, t, T_1, T_2) \cdot A_{m_2,1}(k-k_1, n-n_1, T_1, T_2)]\, e^{i\Omega_{3w} t}\, dk_1. \end{aligned} \tag{27}$$

The right-hand side of equation (27) involves the first and second order amplitude density functions. Using equation (26) to express the second order amplitude density function in terms of the first order amplitude density function, equation (27) may be expressed as

$$\begin{aligned} \frac{\partial A_{m,3}}{\partial t} = & -\frac{\partial A_{m,1}}{\partial T_2} \\ & + \sum_{m_1, m_2} \sum_{n_1} \tilde{I}_2(k, n, m, m_1, m_2, n_1, t, T_1, T_2) \\ & + \sum_{m_1, m_2} \sum_{m_3, m_4} \sum_{n_1, n_2} \cdot \tilde{I}_3(k, n, m, m_1, m_2, m_3, m_4, n_1, n_2, t, T_1, T_2) \end{aligned} \tag{28}$$

where

$$\tilde{I}_2 = \int_{-\infty}^{\infty} \tilde{b} A_{m_1,1}(k_1, n_1, T_1, T_2) \cdot A_{m_2,1}(k-k_1, n-n_1, T_1, T_2)\, e^{i\Omega_{3w} t}\, dk_1$$

$$\tilde{I}_3 = \int_{-\infty}^{\infty} \int_{-\infty}^{\infty} \tilde{c} A_{m_1,1}(k_1, n_1, T_1, T_2) \cdot A_{m_3,1}(k_2, n_2, T_1, T_2) \cdot A_{m_4,1}(k-k_1-k_2, n-n_1-n_2, T_1, T_2) \cdot e^{i\Omega_{4w} t}\, dk_1\, dk_2$$

$$\tilde{b} = b^T \frac{[a_{m_1}(k_1, n_1) + a_{m_2}(k-k_1, n-n_1) - a_m(k,n)]}{i\Omega_{3w}}$$

$$\begin{aligned} \tilde{c} = & [b^T(k_1, k-k_1, n_1, n-n_1, m_1, m_2, m) \\ & + b^T(k-k_1, k_1, n-n_1, n_1, m_2, m_1, m)] \\ & \cdot \frac{b^S(k_2, k-k_1-k_2, n_2, n-n_1-n_2, m_3, m_4, m_2)}{i\Omega_{3w}} \\ & + [b(k_1, k-k_1, n_1, n-n_1, m_1, m_2, m) \\ & + b(k-k_1, k_1, n-n_1, n_1, m_2, m_1, m)] \\ & \cdot \frac{b^T(k_2, k-k_1-k_2, n_2, n-n_1-n_2, m_3, m_4, m_2)}{i\Omega_{3w}} \end{aligned}$$

and

$$\begin{aligned} \Omega_{4w} &= \Omega_{3w}(k, n, m, k_1, n_1, m_1, m_2) \\ &\quad + \Omega_{3w}(k-k_1, n-n_1, m_2, k_2, n_2, m_3, m_4) \\ &= \omega_m^R(k,n) - \omega_{m_1}^R(k_1, n_1) \\ &\quad - \omega_{m_3}^R(k_2, n_2) - \omega_{m_4}^R(k-k_1-k_2, n-n_1-n_2). \end{aligned}$$

The forcing function on the right-hand side of equation (28) contains two integrals. The first integral has a form similar to the integral in equation (23). The second integral involves an integrand which oscillates on the fast time scale with a frequency Ω_{4w}. If the dispersion relation allows a four-wave resonance, there are points in the wavenumber space where $\Omega_{4w} = 0$. When this condition is satisfied, the integrand does not depend on the fast time scale. Thus, as in the case of the second order equations, the forcing functions on the right-hand side of equation (28) may be split into a "steady" part and an oscillatory part.

Application of the solvability condition results in the following equation describing the evolution of the leading order amplitude density function on the T_2 time scale:

$$\frac{\partial A_{m,1}}{\partial T_2} = \sum_{m_1,m_2}\sum_{n_1} \tilde{I}_2^{\mathrm{S}}(k,n,m,m_1,m_2,n_1,T_1,T_2) + \sum_{\substack{m_1,m_2\\m_3,m_4}}\sum_{n_1,n_2} \cdot \tilde{I}_3^{\mathrm{S}}(k,n,m,m_1,m_2,m_3,m_4,n_1,n_2,T_1,T_2) \tag{29}$$

where $\tilde{I}_2^{\mathrm{S}}$ and $\tilde{I}_3^{\mathrm{S}}$ are the steady parts of the integrals $\tilde{I}_2$ and $\tilde{I}_3$, respectively. $\tilde{I}_2^{\mathrm{S}}$ is determined by contributions from the neighborhood of points satisfying the three-wave resonance condition, as explained earlier. $\tilde{I}_3^{\mathrm{S}}$ is determined by contributions from the neighborhood of points satisfying the four-wave resonance condition $\Omega_{4w} = 0$, and is determined in a similar manner. Quartets of wavenumbers (k_1, n_1), (k_2, n_2), $(k-k_1-k_2, n-n_1-n_2)$ and (k,n) which satisfy this condition, called resonant quartets, exchange a significant amount of energy on the T_2 time scale.

Equations (24) and (29) may be combined to yield a single equation for the evolution of the leading order amplitude density function:

$$\frac{\partial A_{m,1}}{\partial T} = a_m A_{m,1} + \sum_{m_1,m_2}\sum_{n_1} \tilde{I}_4^{\mathrm{S}}(k,n,m,m_1,m_2,n_1,T) + \sum_{\substack{m_1,m_2\\m_3,m_4}}\sum_{n_1,n_2} \cdot \tilde{I}_5^{\mathrm{S}}(k,n,m,m_1,m_2,m_3,m_4,n_1,n_2,T) \tag{30}$$

where $T = \varepsilon t$ and $\tilde{I}_4^{\mathrm{S}}$ and $\tilde{I}_5^{\mathrm{S}}$ are the steady parts of the integrals

$$\tilde{I}_4 = \int_{-\infty}^{\infty} [b+\varepsilon\tilde{b}] A_{m_1,1}(k_1,n_1,T) \cdot A_{m_2,1}(k-k_1,n-n_1,T)\, \mathrm{e}^{i\Omega_{3w}t}\, \mathrm{d}k_1$$

and

$$\tilde{I}_5 = \int\int_{-\infty}^{\infty} \varepsilon\tilde{c} A_{m_1,1}(k_1,n_1,T) A_{m_3,1}(k_2,n_2,T) \cdot A_{m_4,1}(k-k_1-k_2,n-n_1-n_2,T)\, \mathrm{e}^{i\Omega_{4w}t}\, \mathrm{d}k_1\, \mathrm{d}k_2$$

respectively. Equation (30) is the generalization of the weakly nonlinear interaction of stationary waves of a continuous spectrum [13] to travelling waves.

It is worthwhile to note that the eigenfunction expansion (13) implies the following expansion for the disturbance quantities

$$\hat{U}_j(k,n,r,t) = \varepsilon\hat{U}_{1j}(k,n,r,t,T_1,T_2) + \varepsilon^2\hat{U}_{2j} + \varepsilon^3\hat{U}_{3j} + \dots \tag{31}$$

The first order perturbation quantities are given by

$$\hat{U}_{1j} = \sum_{m=1}^{\infty} A_{m,1}\tilde{U}_{mj}\, \mathrm{e}^{-i\omega_m^{\mathrm{R}}t} \tag{32}$$

where $\tilde{U}_{mj}$ is the jth component of the vector $\tilde{\mathbf{U}}_m$. The second order perturbation quantities are given by

$$\hat{U}_{2j} = \sum_{m=1}^{\infty}\sum_{m_1,m_2}\sum_{n_1}\int_{-\infty}^{\infty} b^{\mathrm{T}} A_{m_1,1}(k_1,n_1,T_1,T_2) \cdot A_{m_2,1}(k-k_1,n-n_1,T_1,T_2) \cdot \frac{\mathrm{e}^{-i[\omega_{m_1}^{\mathrm{R}}(k_1,n_1)+\omega_{m_2}^{\mathrm{R}}(k-k_1,n-n_1)]t}}{i\Omega_{3w}}\tilde{U}_{mj}\, \mathrm{d}k_1. \tag{33}$$

Equation (33) indicates that even if we consider only the least stable eigenmode ($m = 1$) at leading order, nonlinear interactions excite an infinite number of eigenmodes at second order since the interaction coefficients are non-zero for the higher modes ($m \geqslant 2$), although the infinite sum over the eigenmodes m_1 and m_2 in equation (33) now reduces to only one term. Classical weakly nonlinear theories take this into account by solving the perturbation equations for the second harmonic and the mean-flow distortion at second order directly without using an eigenfunction expansion. In order to make a comparison with classical weakly nonlinear theories, we solve the Navier–Stokes equations by a perturbation method first in the following section.

2.4.2. *Perturbation and expansion.* In the section, we follow the lead of Stuart [1], and solve the Navier–Stokes equations (5) by a perturbation method before using the eigenfunction expansion. The dependent variables are expanded in a perturbation series as follows

$$\hat{\mathbf{U}}(k,n,r,t) = \varepsilon\hat{\mathbf{U}}_1(k,n,r,t,T_1,T_2) + \varepsilon^2\hat{\mathbf{U}}_2 + \varepsilon^3\hat{\mathbf{U}}_3 + \dots \tag{34}$$

The first order perturbation quantities are solutions of the linearized disturbance equations (12). They may be expressed in the form

$$\hat{\mathbf{U}}_1(k,n,r,t,T_1,T_2) = \sum_{m=1}^{M} B_m(k,n,T_1,T_2)\tilde{\mathbf{U}}_m(k,n,r)\, \mathrm{e}^{-i\omega_m^{\mathrm{R}}t} \tag{35}$$

where $B_m(k,n,T_1,T_2)$ is a slowly-varying amplitude density function of order one. We have kept M eigenmodes in equation (35). In the limit as M approaches infinity, the results of this section become the same as the results of Section 2.4.1. The weakly nonlinear theory of monochromatic waves [1] considers only the least stable eigenmode at this order. We can recover the result of classical weakly nonlinear theory by setting M to one. A comparison of equations (32) and (35) reveals that the relation between the two expansions is given by $B_m = A_{m,1}$.

The second order perturbation quantities are described by the equations

$$D\hat{u}_2(k,n,r)+\frac{\hat{u}_2(k,n,r)}{r}+\frac{in\hat{v}_2(k,n,r)}{r}+ik\hat{w}_2(k,n,r)=0$$

$$\frac{\partial \tilde{U}_{2j}}{\partial t}+L_j(k,n,\hat{\mathbf{U}}_2,\hat{P}_2)=-\sum_{m=1}^{M}\left[\frac{\partial B_m}{\partial T_1}-a_m(k,n)B_m\right]\tilde{U}_{mj}\,e^{-i\omega_m^R t}-\hat{N}_{2j} \quad (36)$$

where

$$\hat{N}_{2j}=-\sum_{m_1=1}^{M}\sum_{m_2=1}^{M}\sum_{n_1=-\infty}^{\infty}\int_{-\infty}^{\infty}B_{m_1}(k_1,n_1)\cdot B_{m_2}(k-k_1,n-n_1)M_j(k,n,\tilde{\mathbf{U}}_{m_1},\tilde{\mathbf{U}}_{m_2})\cdot e^{-i[\omega_{m_1}^R(k_1,n_1)+\omega_{m_2}^R(k-k_1,n-n_1)]t}\,dk_1.$$

Application of the Fredholm alternative theory leads to the following equation describing the evolution of the amplitude density function on the T_1 time scale:

$$\frac{\partial B_m}{\partial T_1}=a_m B_m+\sum_{m_1=1}^{M}\sum_{m_2=1}^{M}\sum_{n_1=-\infty}^{\infty}\cdot I_1^S(k,n,m,m_1,m_2,n_1,T_1,T_2) \quad (37)$$

where I_1^S is the steady part of the integral

$$I_1=\int_{-\infty}^{\infty}bB_{m_1}(k_1,n_1)B_{m_2}(k-k_1,n-n_1)\,e^{i\Omega_{3w}t}\,dk_1.$$

It is worth noting that equation (37) is identical to equation (24).

Equations (36) may be solved by using the method of eigenfunction expansion after substituting equation (37) into the right hand side. This yields the solution (33). However, the series (33) may converge slowly because, as noted earlier, a single eigenmode at first order may excite a large number of eigenmodes at second order through nonlinear interactions. In this section, the solution to the second order equations (36) is expressed in the form

$$\hat{\mathbf{U}}_2=\sum_{m_1=1}^{M}\sum_{m_2=1}^{M}\sum_{n_1=-\infty}^{\infty}\cdot\int_{-\infty}^{\infty}B_{m_1}(k_1,n_1)B_{m_2}(k-k_1,n-n_1)\cdot\tilde{\mathbf{U}}_2(m_1,m_2,k_1,k-k_1,n_1,n-n_1,r)\cdot e^{-i[\omega_{m_1}^R(k_1,n_1)+\omega_{m_2}^R(k-k_1,n-n_1)]t}\,dk_1 \quad (38)$$

where the functions $\tilde{\mathbf{U}}_2=(\tilde{\hat{u}}_2,\tilde{\hat{v}}_2,\tilde{\hat{w}}_2,\tilde{\hat{\theta}}_2)$ are independent of the amplitude density function B_m and can be determined by solving the following system of equations:

$$D\tilde{\hat{u}}_2+\frac{\tilde{\hat{u}}_2}{r}+\frac{in\tilde{\hat{v}}_2}{r}+ik\tilde{\hat{w}}_2=0,$$

$$L_j(k,n,\tilde{\hat{\mathbf{U}}}_2,\tilde{\hat{p}}_2)-i[\omega_{m_1}^R(k_1,n_1)+\omega_{m_2}^R(k-k_1,n-n_1)]\tilde{\hat{U}}_{2j}=-M_j(k,n,\tilde{U}_{m_1}(k_1,n_1,r),\tilde{U}_{m_2}(k-k_1,n-n_1,r))+\sum_{m=1}^{M}b^S\tilde{U}_{mj}. \quad (39)$$

Since the series solution (33) may converge slowly, it may be advantageous to solve the equations (37) directly using a numerical method.

The disturbance field at third order is described by the equations

$$D\hat{u}_3+\frac{\hat{u}_3}{r}+\frac{in\hat{v}_3}{r}+ik\hat{w}_3=0$$

$$\frac{\partial \hat{U}_{3j}}{\partial t}+L_j(k,n,\hat{\mathbf{U}}_3,\hat{P}_3)=-\sum_{m=1}^{M}\frac{\partial B_m}{\partial T_2}\tilde{U}_{mj}\,e^{-i\omega_m^R t}-\hat{N}_{3j} \quad (40)$$

where

$$\hat{N}_{3j}=\sum_{m_1=1}^{M}\sum_{m_2=1}^{M}\sum_{n_1=-\infty}^{\infty}\cdot\int_{-\infty}^{\infty}B_{m_1}(k_1,n_1)B_{m_2}(k-k_1,n-n_1)\cdot F_j(m_1,m_2,k_1,k-k_1,n_1,n-n_1,r)\cdot e^{-i[\omega_{m_1}^R(k_1,n_1)+\omega_{m_2}^R(k-k_1,n-n_1)]t}\,dk_1+\sum_{m_1=1}^{M}\sum_{m_2=1}^{M}\sum_{m_3=1}^{M}\sum_{n_1=-\infty}^{\infty}\sum_{n_2=-\infty}^{\infty}\cdot\int_{-a}^{\int}B_{m_1}(k_1,n_1)B_{m_2}(k_2,n_2)\cdot B_{m_3}(k-k_1-k_2,n-n_1-n_2)\cdot G_j(m_1,m_2,m_3,k_1,k_2,k-k_1-k_2,n_1,n_2,n-n_1-n_2,r)\cdot e^{-i[\omega_{m_1}^R(k_1,n_1)+\omega_{m_2}^R(k_2,n_2)+\omega_{m_3}^R(k-k_1-k_2,n-n_1-n_2)]t}\,dk_1\,dk_2$$

where the inertial forcing functions F_j and G_j depend on the linear stability eigenfunctions and the functions determined at second order. They are

$$F_j=[a_{m_1}(k_1,n_1)+a_{m_2}(k_2,n_2)]\tilde{\hat{U}}_{2j},$$

$$G_1=2D[\tilde{u}_{m_1}\tilde{\hat{u}}_2]+\frac{2}{r}[\tilde{u}_{m_1}\tilde{\hat{u}}_2-\tilde{v}_{m_1}\tilde{\hat{v}}_2]+\frac{i2n}{r}[\tilde{u}_{m_1}\tilde{\hat{v}}_2+\tilde{v}_{m_1}\tilde{\hat{u}}_2]+i2k[\tilde{u}_{m_1}\tilde{\hat{w}}_2+\tilde{w}_{m_1}\tilde{\hat{u}}_2]+\sum_{m=1}^{M}b^s[\tilde{\hat{u}}_2(m_1,m,k_1,k_2+k_3,n_1,n_2+n_3,r)+\tilde{\hat{u}}_2(m,m_1,k_2+k_3,k_1,n_2+n_3,n_1,r)]$$

$$G_2 = D[\tilde{u}_{m_1}\tilde{\tilde{v}}_2 + \tilde{v}_{m_1}\tilde{\tilde{u}}_2] + \frac{2}{r}[\tilde{u}_{m_1}\tilde{\tilde{v}}_2 + \tilde{v}_{m_1}\tilde{\tilde{u}}_2]$$
$$+ \frac{i4n}{r}\tilde{v}_{m_1}\tilde{\tilde{v}}_2 + i2k[\tilde{v}_{m_1}\tilde{\tilde{w}}_2 + \tilde{w}_{m_1}\tilde{\tilde{v}}_2]$$
$$+ \sum_{m=1}^{M} b^s[\tilde{\tilde{v}}_2(m_1, m, k_1, k_2+k_3, n_1, n_2+n_3, r)$$
$$+ \tilde{\tilde{v}}_2(m, m_1, k_2+k_3, k_1, n_2+n_3, n_1, r)]$$
$$G_3 = D[\tilde{u}_{m_1}\tilde{\tilde{w}}_2 + \tilde{w}_{m_1}\tilde{\tilde{u}}_2]$$
$$+ \frac{in}{r}[\tilde{u}_{m_1}\tilde{\tilde{w}}_2 + \tilde{w}_{m_1}\tilde{\tilde{u}}_2] + i4k\tilde{w}_{m_1}\tilde{\tilde{w}}_2$$
$$+ \sum_{m=1}^{M} b^s[\tilde{\tilde{w}}_2(m_1, m, k_1, k_2+k_3, n_1, n_2+n_3, r)$$
$$+ \tilde{\tilde{w}}_2(m, m_1, k_2+k_3, k_1, n_2+n_3, n_1, r)],$$
$$G_4 = D[\tilde{u}_{m_1}\tilde{\tilde{\theta}}_2 + \tilde{\theta}_{m_1}\tilde{\tilde{u}}_2]$$
$$+ \frac{1}{r}[\tilde{u}_{m_1}\tilde{\tilde{\theta}}_2 + \tilde{\theta}_{m_1}\tilde{\tilde{u}}_2] + i2n[\tilde{v}_{m_1}\tilde{\tilde{\theta}}_2 + \tilde{\theta}_{m_1}\tilde{\tilde{v}}_2]$$
$$+ \sum_{m=1}^{M} b^s[\tilde{\tilde{\theta}}_2(m_1, m, k_1, k_2+k_3, n_1, n_2+n_3, r)$$
$$+ \tilde{\tilde{\theta}}_2(m, m_1, k_2+k_3, k_1, n_2+n_3, n_1, r)].$$

Application of the Fredholm alternative theory yields an equation describing the evolution of the amplitude density function on the T_2 time scale

$$\frac{\partial B_m}{\partial T_2} = \sum_{m_1=1}^{M}\sum_{m_2=1}^{M}\sum_{n_1=-\infty}^{\infty} \cdot I_2^S(k, n, m, m_1, m_2, n_1, T_1, T_2)$$
$$+ \sum_{m_1=1}^{M}\sum_{m_2=1}^{M}\sum_{m_3=1}^{M}\sum_{n_1=-\infty}^{\infty}\sum_{n_2=-\infty}^{\infty} \cdot I_3^S(k, n, m_1, m_2, m_3, n_1, n_2, T_1, T_2) \quad (41)$$

where I_2^S and I_3^S denote the steady parts of the integrals

$$I_2 = \int_{-\infty}^{\infty} \hat{b} B_{m_1}(k_1, n_1) B_{m_2}(k-k_1, n-n_1)\, e^{i\Omega_{3w}t}\, dk_1$$

and

$$I_3 = \int_{-\infty}^{\infty}\int_{-\infty}^{\infty} \hat{c} B_{m_1}(k_1, n_1) B_{m_2}(k_2, n_2) B_{m_3} \cdot (k-k_1-k_2, n-n_1-n_2)\, e^{i\Omega_{4w}t}\, dk_1\, dk_2.$$

The interaction coefficients are $\hat{b} = \langle \mathbf{U}_m^\dagger, \mathbf{F}\rangle$, and $\hat{c} = \langle \mathbf{U}_m^\dagger, \mathbf{G}\rangle$. Equation (41) has a form similar to equation (29). However, the interaction coefficients $\hat{b}$ and $\hat{c}$ in the integrals I_2 and I_3 are evaluated in terms of the eigenfunctions $\tilde{\mathbf{U}}_{m_1}$ of the linearized equations (12) and the functions $\tilde{\tilde{\mathbf{U}}}_2$ are determined from the second order equations (39). The coefficients $\tilde{b}$ and $\tilde{c}$ in the integrals $\tilde{I}_2$ and $\tilde{I}_3$, on the other hand, are expressed only in terms eigenfunctions $\tilde{\mathbf{U}}_m$ of linear stability theory.

The equations (37) and (41) obtained at second and third orders respectively may be combined to yield a single equation for the evolution of the amplitude density function

$$\frac{\partial B_m}{\partial T} = a_m B_m + \sum_{m_1, m_2}\sum_{n_1} I_4^S(k, n, m, m_1, m_2, n_1, T)$$
$$+ \sum_{m_1, m_2, m_3}\sum_{n_1, n_2} I_5^S(k, n, m, m_1, m_2, m_3, n_1, n_2, T) \quad (42)$$

where I_4^S and I_5^S are the steady parts of the integrals

$$I_4 = \int_{-\infty}^{\infty} [b + \varepsilon\hat{b}] B_{m_1}(k_1, n_1) B_{m_2} \cdot (k-k_1, n-n_1)\, e^{i\Omega_{3w}t}\, dk_1$$

and

$$I_5 = \int_{-\infty}^{\infty}\int_{-\infty}^{\infty} \varepsilon\hat{c} B_{m_1}(k_1, n_1) B_{m_2}(k_2, n_2) B_{m_3} \cdot (k-k_1-k_2, n-n_1-n_2)\, e^{i\Omega_{4w}t}\, dk_1\, dk_2$$

respectively. Equation (42) is equivalent to the equation (30) derived in Section 2.4.1. The amplitude density function B_m is equivalent to the first order amplitude density function $A_{m,1}$ of Section 2.3. If we consider only the interactions of the least stable eigenmodes for each wave-component, that is, if we set $M = 1$, equation (42) simplifies to

$$\frac{\partial B_1}{\partial T} = a_1 B_1 + \sum_{n_1} I_4^S(k, n, 1, 1, 1, n_1, T) + \sum_{n_1, n_2} I_5^S(k, n, 1, 1, 1, 1, n_1, n_2, T). \quad (43)$$

In the special case when $\omega_m^R \equiv 0$, equation (43) reduces to the integro-differential equation for the amplitude density function of a continuous spectrum of stationary waves derived previously by Yao and Ghosh Moulic [13].

2.4.3. *Monochromatic waves and slowly-varying wavepackets.* The equation (30) for the evolution of the amplitude density function of a continuous spectrum contains as a special case the equation describing the evolution of the amplitude of a discrete monochromatic wave. The amplitude density function for a discrete wave with axial wavenumber k_0 and azimuthal wavenumber n_0 may be expressed in the form

$$A_{m,1}(k, n, t) = [A_0(t)\delta(k-k_0)\delta_{n,n_0} + A_0^*(t)\delta(k+k_0)\delta_{n,-n_0}]\delta_{m,1} \quad (44)$$

where $\delta(k)$ represents the Dirac delta function, $\delta_{i,j}$ represents the Kronecker delta, and the asterisk denotes complex conjugates. We have retained only the least stable mode ($m = 1$) in the leading order amplitude density function expressed in equation (44).

Substitution of equation (44) into equation (30) leads to

$$\frac{dA_0}{dt} = a_0 A_0 + a_1 |A_0|^2 A_0 \tag{45}$$

where $a_0 = \omega_1^1(k_0, n_0)$ is the amplification rate predicted by linear stability theory for the least stable eigenmode of the wavenumber $(k_0 n_0)$ and

$$\begin{aligned} a_1 = {} & \hat{c}(k_0, -k_0, k_0, n_0, -n_0, n_0, 1, 1, 1, 1) \\ & + \hat{c}(-k_0, k_0, k_0, -n_0, n_0, n_0, 1, 1, 1, 1) \\ & + \hat{c}(k_0, k_0, -k_0, n_0, n_0, -n_0, 1, 1, 1, 1) \end{aligned} \tag{46}$$

is the second Landau constant. Equation (45) is the Landau equation describing the temporal evolution of the amplitude of a monochromatic wave [1]. Equation (30) for the evolution of the amplitude density function of a continuous spectrum can also be reduced to a set of N ordinary differential equations describing the evolution of the amplitude of N discrete waves [35].

It is worth noting that, although equation (30) describes the temporal evolution of the amplitude density function in wave space, the integral formulation does include spatial variations of the disturbances through the Fourier integral transform (4), and is not restricted to periodic disturbances. In the special case of a slowly-varying wavepacket, the Ginzburg–Landau equation, with an azimuthal wavenumber n_0, and a spectrum confined to a small neighbourhood of bandwidth δ around the minimum critical wavenumber k_c, equation (4) becomes

$$w'(r, \phi, z, t) = \tilde{A}(k_c, n_0, z, t) \tilde{w}_1(k_c, n_0, r) \cdot e^{i[k_c z + n_0 \phi - \omega_1^R(k_c, n_0) t]} + c \cdot c. \tag{47}$$

where

$$\begin{aligned} \tilde{A}(k_c, n_0, z, t) &= \int_{k_c - \delta}^{k_c + \delta} A_1(k, n_0, t) \cdot e^{i(k - k_c) z + i[\omega_1^R(k_c, n_0) - \omega_1^R(k, n_0)] t} \, dk \\ &= \varepsilon \int_{-\delta/\varepsilon}^{\delta/\varepsilon} A_1(k_c + \varepsilon K, n_0, t) \cdot e^{i\varepsilon K z + i[\omega_1^R(k_c, n_0) - \omega_1^R(k_c + \varepsilon K, n_0)] t} \, dK \end{aligned} \tag{48}$$

is the slowly-varying envelope of the wavetrain and $c \cdot c.$ denotes the complex conjugate. As in equation (44), we have retained only the least stable mode $(m = 1)$ in equation (48). In order to derive an equation for the envelope of the wavepacket, we multiply equation (30) by $e^{i(k - k_c) z + i[\omega_1^R(k_c, n_0) - \omega_1^R(k, n_0)] t} \delta_{n, n_0} \delta_{m, 1}$ and integrate with respect to k from $k_c - \delta$ to $k_c + \delta$. We expand the linear amplification rates and frequencies in a Taylor series around $k = k_c$:

$$a(k, n_0) = a(k_c, n_0) + \frac{1}{2} \frac{d^2 a}{dk^2}(k_c, n_0)(k - k_c)^2 + \ldots \tag{49}$$

and

$$\omega^R(k, n_0) = \omega^R(k_c, n_0) + \frac{d\omega^R}{dk}(k_c, n_0)(k - k_c) + \ldots$$

It may be noted that, at the minimum critical wavenumber k_c, $(da/dk)(k_c, n_0) = 0$. With equations (48) and (49), in the limit as $\varepsilon \to 0$, it can be shown that equation (20) reduces to the equation describing the spatio-temporal evolution of a wavepacket derived by Stewartson and Stuart [3]:

$$\left(\frac{\partial}{\partial t} + c_g \frac{\partial}{\partial z} \right) \tilde{A} = a_0 \tilde{A} + a_2 \frac{\partial^2}{\partial z^2} \tilde{A} + a_1 |\tilde{A}|^2 \tilde{A} \tag{50}$$

where $a_2 = -\frac{1}{2}(d^2 a/dk^2)(k_c, n_0)$ and $c_g = (d\omega^R/k)(k_c, n_0)$ is the group velocity. In the special case when the group velocity is zero, equation (50) reduces to the equation for thermal convection derived by Newell and Whitehead [4] and Segel [5].

It is worth pointing out that there are no combinations of wavenumbers involving only the waves $\pm k_0$, which form a resonant triad. Thus, in the above limiting cases of monochromatic waves, and wavepackets with one dominant wavenumber, there is no contribution from the integrals $\tilde{I}_4^S$ in equation (30). Also, the nonlinear term in equation (50) which leads to an exchange of energy among the wave components is identical to that for monochromatic waves in (45). This shows that there is no energy transfer among the wave components in a wavepacket. Equation (30), on the other hand, allows nonlinear exchange of energy among the wave components of a continuous band of waves with widely differing wavenumbers. The advantage of this formulation are that it is simpler than previous theories and contains information on temporal and spatial evolution of nonlinear, interacting monochromatic waves, wave trains, and waves of a continuous spectrum.

Both the Landau equation and the Ginzburg–Landau equation assume that the deformation of the mean flow is at a smaller order than that of the dominant wave. Yao and Ghosh Moulic [13] demonstrated that a formulation without considering the leading-order effect of the mean-flow deformation fails to account for the proper energy exchange among the disturbance waves and the mean flow.

3. RESULTS AND DISCUSSION

The velocity and temperature distributions can be determined by integrating the amplitude density function. The axial velocity component is given by

$$w(r, \phi, z, t) = W_0(r) + \int_{-\infty}^{\infty} \sum_{n=-\infty}^{\infty} \sum_{m=1}^{\infty} \cdot A_m(k, n, t) \tilde{w}_m(k, n, r) \, e^{i(kz + n\phi)} \, dk \tag{51}$$

where A_m is the amplitude density function obtained by solving the set of integro-differential equations (15). Similar expressions may be written for the other velocity components. The weakly nonlinear expansion

for the axial velocity component may be summarized in the form

$$
\begin{aligned}
w(r,\phi,z,t) &= W_0(r)+\varepsilon\sum_m\sum_n \\
&\cdot\int_{-\infty}^{\infty} B_m(k,n,T_1,T_2)\tilde{w}_m(k,n,r) \\
&\cdot e^{i(kz+n\phi-\omega_m^R(k,n)t)}\,dk+\varepsilon^2\sum_{m_1,m_2}\sum_{n_1}\sum_{n}\int_{-\infty}^{\infty}\int_{-\infty}^{\infty} \\
&\cdot B_{m_1}(k_1,n_1,T_1,T_2)B_{m_2}(k-k_1,n-n_1,T_1,T_2) \\
&\cdot\tilde{w}_2(m_1,m_2,k_1,k-k_1,n_1,n-n_1,r) \\
&\cdot e^{ikz+in\phi-i[\omega_{m_1}^R(k_1,n_1)+\omega_{m_2}^R(k-k_1,n-n_1)]t}\,dk_1\,dk \\
&+\varepsilon^3\sum_{m_1,m_2,m_3}\sum_{n_1,n_2}\sum_{n}\int_{-\infty}^{\infty}\int_{-\infty}^{\infty}\int_{-\infty}^{\infty} \\
&\cdot B_{m_1}(k_1,n_1)B_{m_2}(k_2,n_2) \\
&\cdot B_{m_3}(k-k_1-k_2,n-n_1-n_2) \\
&\tilde{w}_3(m_1,m_2,m_3,k_1,k_2,k-k_1 \\
&-k_2,n_1,n_2,n-n_1-n_2,r) \\
&e^{ikz+inf-i[\omega_{m_1}^R(k_1,n_1)+\omega_{m_2}^R(k_2,n_2)+\omega_{m_3}^R(k-k_1-k_2,n-n_1-n_2)]t}\,dk_1\,dk_2\,dk \\
&+\ldots \qquad (52)
\end{aligned}
$$

where B_m is obtained by solving the set of integro-differential equations (42).

Numerical results have been obtained for an annulus with a radius ratio $\eta = 0.375$, $Re = 1000$, $Pr = 6$ and three Rayleigh numbers $Ra = 90$, 100 and 200. The critical Rayleigh number at the onset of instability for this flow configuration is $Ra_c = 89$ [10]. The critical wavenumber is $k_c = 0.3$. Linear stability analysis indicates that, at $Ra = 200$, the parallel basic flow is unstable to disturbances with wavenumbers lying between 0.23 and 1.13. The maximum amplification rate predicted by linear stability analysis at $Ra = 200$ is $\varepsilon = 0.0043$. The values of ε at $Ra = 100$ and $Ra = 90$ are 0.00048 and 0.00031, respectively. The integro-differential equation (15) for the evolution of the amplitude density function was solved numerically using 20 terms in the eigenfunction expansion. Equation (43) representing weakly nonlinear interactions among the *least stable* eigenmodes for each wave component of a continuous spectrum was also solved numerically. The integrals in equation (15) were discretized by the trapezoidal rule using a uniform mesh size $\Delta k = 0.25$. The infinite range of integration was truncated to $-3 \leqslant k \leqslant 3$, which was found to be adequate as the kinetic energies of the high wavenumber modes were negligible. The nonlinear terms in equation (15) were evaluated pseudospectrally using fast Fourier transforms. Aliasing errors resulting from pseudospectral evaluation of the convolution sums were eliminated by padding using the two-third rule [12]. The computations were performed on the CRAY C-90 supercomputer at the Pittsburgh Supercomputer Center. Within the range of selected flow parameters, the flow is linearly stable to asymmetric disturbances and no azimuthal modes were found to be excited in the direct numerical simulations [12]. In order to reduce the computer time, the computations presented in this section were done for the axisymmetric case.

The integro-differential equation (15) was solved with different initial conditions. Results for four initial conditions are presented in this section. In all cases, the final equilibrium state was found to be a monochromatic travelling wave with a single dominant mode with wavenumber k_f and its superharmonics of smaller amplitudes. The phase speed $c_m(k,n)$ for each eigenmode, defined by

$$c_m = -\frac{1}{k}\frac{d\beta_m}{dt} \qquad (53)$$

was computed, where $\beta_m(k,n)$ is the phase angle given by equation (18). In the initial stages of the evolution of the waves, the wave amplitudes are small and nonlinear effects are negligible. Thus, in the initial stages of the evolution, the phase speed of the different eigenmodes is close to the value ω_m^R/k predicted by linear stability theory, as indicated by equation (18). The wave-speeds predicted by linear stability theory for different eigenmodes are tabulated for $Ra = 90$, 100 and 200 in Tables 1–3, respectively. As indicated by the tables, there is a large variation in the linear wave-speeds of the different eigenmodes for the same wavenumber. However, in all the cases presented in this section, the equilibrium wave-speeds of all the eigenmodes were found to be the same. Thus, the harmonics of the fundamental wave k_f are phase-locked at equilibrium. The equilibrium wave-speeds c_{eq} for four different equilibrium states are given in Table 4. The values of the equilibrium wave-speeds are close to the linear wave-speeds of the least stable eigenmodes. Thus, the wave-speeds of the least stable eigenmodes are modified only slightly by nonlinear effects. The wave-speeds of the higher eigenmodes, on the other hand, are modified substantially by nonlinear wave interactions.

Figure 2(a) shows the results of a numerical solution of the set of integro-differential equations (15) at $Ra = 200$ in which the initial disturbance consisted of a single dominant mode with wavenumber $k = 0.75$. The evolution of the kinetic energy of the dominant wave components is plotted in Fig. 2(a). For axisymmetric flow, the kinetic energy of the k^{th} Fourier mode is given by

$$E(k,t) = \begin{cases} \displaystyle\int_{r_i}^{r_o} r[|\hat{u}|^2+|\hat{w}|^2]\,dr & k \neq 0 \\ \displaystyle\frac{1}{2}\int_{r_i}^{r_o} r[|W_0+\hat{w}|^2-W_0^2]\,dr & k = 0 \end{cases} \qquad (54)$$

Table 1. Wave-speeds for the different eigenmodes predicted by linear stability theory at $Ra = 200$

m	$k = 0.5$	$k = 0.75$	$k = 1$	$k = 1.5$
1	0.2201E+00	0.2136E+00	0.2112E+00	0.2123E+00
2	0.1987E−01	0.1717E−01	0.1550E−01	0.1343E−01
3	0.1889E+00	0.1942E+00	0.1976E+00	0.1411E+00
4	0.7381E−01	0.6203E−01	0.1418E+00	0.2015E+00
5	0.1511E+00	0.1364E+00	0.5522E−01	0.4720E−01
6	0.1105E+00	0.1554E+00	0.1628E+00	0.1739E+00
7	0.1162E+00	0.9549E−01	0.8561E−01	0.7342E−01
8	0.1285E+00	0.1350E+00	0.1459E+00	0.1558E+00
9	0.1257E+00	0.1234E+00	0.1139E+00	0.9877E−01
10	0.1191E+00	0.1221E+00	0.1274E+00	0.1399E+00
11	0.1249E+00	0.1247E+00	0.1246E+00	0.1203E+00
12	0.1248E+00	0.1247E+00	0.1246E+00	0.1411E+00
13	0.1094E+00	0.1105E+00	0.1115E+00	0.1079E+00
14	0.1247E+00	0.1247E+00	0.1247E+00	0.1253E+00
15	0.1245E+00	0.1245E+00	0.1244E+00	0.1243E+00
16	0.1208E+00	0.1198E+00	0.1183E+00	0.1122E+00
17	0.1244E+00	0.1244E+00	0.1244E+00	0.1240E+00
18	0.1244E+00	0.1245E+00	0.1245E+00	0.1252E+00
19	0.1245E+00	0.1246E+00	0.1248E+00	0.1185E+00
20	0.1168E+00	0.1172E+00	0.1176E+00	0.1257E+00

Table 2. Wave-speeds for the different eigenmodes predicted by linear stability theory at $Ra = 100$

m	$k = 0.3$	$k = 0.6$
1	0.3192E+00	0.3116E+00
2	0.4932E−01	0.3918E−01
3	0.2794E+00	0.2926E+00
4	0.1628E+00	0.1280E+00
5	0.2290E+00	0.2482E+00
6	0.1725E+00	0.2014E+00
7	0.2032E+00	0.2231E+00
8	0.2063E+00	0.1836E+00
9	0.2014E+00	0.2065E+00
10	0.2064E+00	0.1953E+00
11	0.2052E+00	0.2058E+00
12	0.2052E+00	0.2051E+00
13	0.1828E+00	0.1852E+00
14	0.2050E+00	0.2051E+00
15	0.2047E+00	0.2049E+00
16	0.2026E+00	0.2010E+00
17	0.2047E+00	0.2048E+00
18	0.2047E+00	0.2048E+00
19	0.2046E+00	0.2047E+00
20	0.1938E+00	0.1944E+00

Table 3. Wave-speeds for the different eigenmodes predicted by linear stability theory at $Ra = 90$

m	$k = 0.3$	$k = 0.6$
1	0.3375E+00	0.3320E+00
2	0.5390E−01	0.4286E−01
3	0.2990E+00	0.3125E+00
4	0.1773E+00	0.2682E+00
5	0.2481E+00	0.2155E+00
6	0.1841E+00	0.1391E+00
7	0.2198E+00	0.2400E+00
8	0.2219E+00	0.1996E+00
9	0.2175E+00	0.2223E+00
10	0.2223E+00	0.2082E+00
11	0.2210E+00	0.2220E+00
12	0.2209E+00	0.2208E+00
13	0.1973E+00	0.2005E+00
14	0.2207E+00	0.2209E+00
15	0.2205E+00	0.2207E+00
16	0.2186E+00	0.2169E+00
17	0.2204E+00	0.2206E+00
18	0.2204E+00	0.2206E+00
19	0.2204E+00	0.2204E+00
20	0.2090E+00	0.2097E+00

Equation (54) accounts for the energy in both modes $\pm k$. The kinetic energy of the fully-developed flow is subtracted from the mean-flow kinetic energy in (54) so that $E(0, t)$ represents the kinetic energy associated with the mean flow distortion. The mode $k = 0.75$ is linearly unstable, and grows initially at the rate predicted by linear theory. Nonlinear interactions generate the harmonics of the mode $k = 0.75$ and induce a mean flow distortion ($k = 0$). As the amplitude of the mode $k = 0.75$ increases, nonlinear effects become important and alter the growth rate, causing the mode to decay and eventually reach an equilibrium state. The equilibrium state is a monochromatic travelling wave in which the fundamental mode $k = 0.75$ remains the dominant mode, while its superharmonics, generated through nonlinear interaction, have smaller amplitudes. The kinetic energy of the third and fourth harmonics ($k = 2.25$ and $k = 3$) are much smaller than the energies of the fundamental mode ($k = 0.75$) and the second harmonic ($k = 1.5$), and have not been plotted in Fig. 2(a). The kinetic

Table 4. Wave-speeds at equilibrium

Ra	90	100	200	200
k_f	0.3	0.3	0.75	0.5
C_{eq}	0.3376	0.3213	0.2175	0.2239

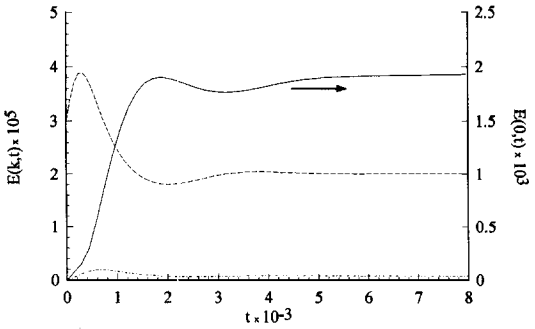

Fig. 2(a). Evolution of the kinetic energy of dominant waves with the initial disturbance at $k = 0.75$. ——, $k = 0$; -----, $k = 0.75$; -·-·-·-·- $k = 1.5$.

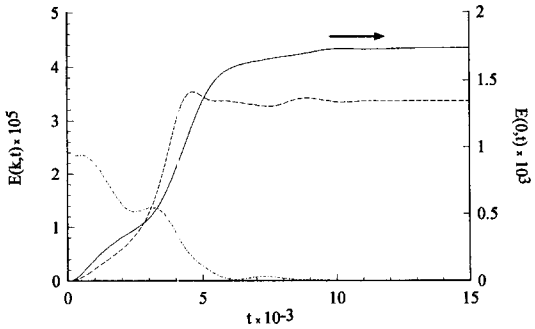

Fig. 2(b). Evolution of the kinetic energy of the dominant waves with the initial disturbance at $k = 0.25$. -·-·-·-·-, $k = 0.25$; ------, $k = 0.5$; ——, $k = 0$.

energy associated with the mean flow distortion ($k = 0$) is higher than the kinetic energy of the fundamental mode $k = 0.75$. This implies that classical weakly nonlinear theories, which assume *a priori* that the order of magnitude of the mean flow distortion is smaller than that of the fundamental wave, are not valid. The results of a direct numerical simulation of the time-dependent Navier–Stokes equations using the spectral method of Fourier–Chebychev expansions starting with the same initial conditions [12] are superimposed on Fig. 2(a). The difference in the two computations cannot be noticed in Fig. 2(a). This is expected since both computations represent exact solutions of the Navier–Stokes equations. The CPU time required for the numerical solution of the set of integrodifferential equations (15) is, however, only 25% of the CPU time required for the direct numerical simulation using a Fourier–Chebyshev spectral method for the current two-dimensional problem. For a three-dimensional problem [36], the savings in CPU time is even more and is a factor of six. The two computer codes were fully optimized to take advantage of the vector facilities on the CRAY C-90 supercomputer. Thus, the relative CPU time for the two computations is a true indication of the computational efficiency of the new algorithm.

Figure 2(b) shows the results of a numerical solution of the set of integro-differential equations (15) at $Ra = 200$ starting with a single dominant mode with wavenumber $k = 0.25$ at time $t = 0$. The mode

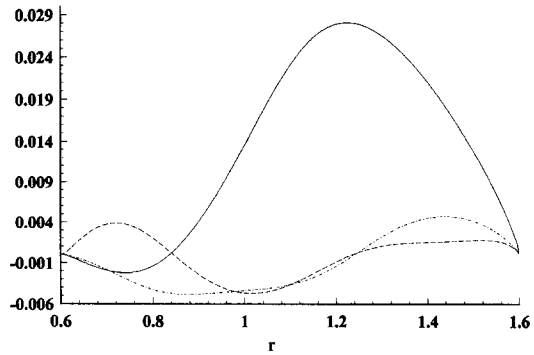

Fig. 3. Axial velocity profiles. ——, Real part for $k = 0.75$; -·-·-·-·-, imaginary for $k = 0.75$; —— $k = 0$.

$k = 0.25$ is linearly unstable at $Ra = 200$ and the weakly nonlinear theory of monochromatic waves predicts a supercritical equilibrium state for this mode. The present computation shows that this equilibrium state is unstable. The mode $k = 0.25$ grows initially and then decays to zero, while its harmonic $k = 0.25$, excited through nonlinear wave interaction, grows and reaches a supercritical equilibrium state. This result is in agreement with the Eckhaus and Benjamin–Feir side-band instability [18]. The results of a direct numerical simulation of the Navier–Stokes equations starting with the same initial conditions [12] cannot be distinguished from the present results in Fig. 2(b), as in the case of Fig. 2(a). The results of Fig. 2(a) and (b) demonstrate that the equilibrium state of the travelling waves is not unique, but depends on the waveform of the initial disturbance.

The velocity and temperature distributions predicted by the numerical solution of the set of integro-differential equations (15) and the direct numerical simulation of the Navier–Stokes equations for the equilibrium state indicated in Fig. 2(a) are compared in Figs. 3 and 4. Figure 3 shows the equilibrium radial shapes of the axial velocity components $\hat{w}(k, n = 0, r)$ for the mean flow distortion ($k = 0$) and the fundamental mode $k = 0.75$, while Fig. 4 shows the corresponding temperature distributions $\hat{\theta}(k, n = 0, r)$. The results of the two computations agree completely

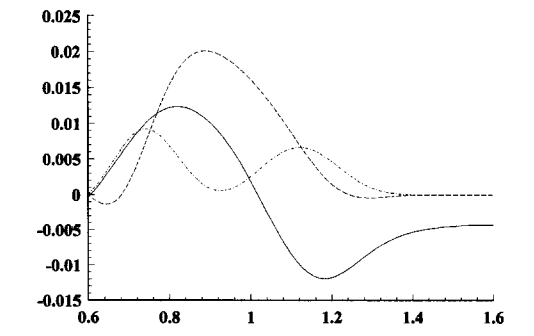

Fig. 4. Temperature distribution. ------, Real part for $k = 0.75$; -·-·-·-·-, imaginary for $k = 0.75$; ——, $k = 0$.

Table 5. Amplitudes of the different eigenmodes for $Ra = 200$ and $k = 0.75$

m	$k = 0$	$k = 0.75$	$k = 1.5$
1	0.1357E−01	0.4490E−02	0.3805E−03
2	0.6223E−02	0.3319E−05	0.1895E−06
3	0.6223E−02	0.6987E−03	0.1659E−03
4	0.9939E−02	0.1137E−03	0.7693E−03
5	0.1728E−02	0.1133E−02	0.5586E−05
6	0.6218E−03	0.7043E−03	0.3546E−03
7	0.6233E−03	0.7334E−03	0.4494E−04
8	0.1509E−03	0.1341E−02	0.1398E−03
9	0.5483E−04	0.1068E−02	0.1736E−03
10	0.2816E−03	0.1401E−03	0.9486E−04
11	0.4112E−04	0.1731E−03	0.2853E−03
12	0.1055E−04	0.4329E−04	0.1156E−03
13	0.7585E−05	0.4539E−04	0.3094E−04
14	0.5969E−05	0.7935E−05	0.1785E−03
15	0.8982E−06	0.1828E−05	0.4256E−04
16	0.1004E−05	0.3327E−04	0.3869E−04
17	0.1176E−04	0.5766E−06	0.6972E−05
18	0.8601E−06	0.3386E−07	0.8432E−06
19	0.1291E−06	0.1443E−06	0.9646E−05
20	0.1629E−06	0.2843E−05	0.5771E−06

and cannot be distinguished in the scale of Figs. 3 and 4.

The equilibrium amplitudes of the eigenmodes, $\bar{R}_m(k) = \Delta k R_m(k, n = 0)$, where $R_m(k, n) = |A_m(k, n)|$ is the magnitude of the complex amplitude density function $A_m(k, n)$ are given in Table 5 for the equilibrium state indicated in Fig. 2(a) at $Ra = 200$. Table 5 shows that amplitude of the least stable eigenmode ($m = 1$) for the fundamental wave $k = 0.75$ is larger than the amplitudes of the other eigenmodes for $k = 0.75$. The amplitudes of the different eigenmodes do not decrease in magnitude monotonically as m increases. For instance, the amplitude of the 5th eigenmode ($m = 5$) for the fundamental wave $k = 0.75$ is higher than the amplitudes of the 2nd, 3rd and 4th eigenmodes. This may be explained by referring to Table 6 which shows the nonlinear terms for the various eigenmodes. Table 6 lists the integrals $\overline{I_m^r}(k) = \Delta k I_m^r(k, n = 0)$, where $\overline{I_m^r}(k)$ is the integral representing energy transfer through nonlinear interactions, defined in equation (17). A glance at Table 6 reveals that $\overline{I_m^r}(k)$ is negative for the first eigenmode of the fundamental wave $k = 0.75$ (which is linearly unstable), and positive for all the other eigenmodes (which are linearly stable). Thus, energy is transferred from the least stable eigenmode of the fundamental wave $k = 0.75$ to the other eigenmodes through nonlinear interactions. The nonlinear term corresponding to the 5th eigenmode for $k = 0.75$ is higher than the corresponding nonlinear terms for the 2nd, 3rd and 4th eigenmodes for $k = 0.75$. Thus, more energy is transferred to the 5th eigenmode, causing it to have a higher amplitude. It may be noted that classical weakly nonlinear theories consider only the least stable eigenmode ($m = 1$) for the fundamental wave at leading order. The amplitudes of the other eigenmodes of the fundamental wave are assumed to be two orders of magnitude lower. However, Table 5 indicates that the amplitudes of the 5th, 8th and 9th eigenmodes for the fundamental wave are of the same magnitude as the amplitude of the least stable mode. Thus, the prediction of classical weakly nonlinear theories does not agree with the exact solution at this Rayleigh number. Table 5 also indicates that the amplitude of the least stable eigenmode for the mean flow distortion ($k = 0$) is higher than the amplitudes of the higher eigenmodes for $k = 0$. However, the amplitudes of the first five eigenmodes for the mean flow distortion are of the same order of magnitude. In the case of the second harmonic ($k = 1.5$), the amplitude of the 4th eigenmode is higher than the least stable eigenmode. Thus, the assumption that the least stable eigenmode is the dominant eigenmode for all the waves is not valid for this case. Table 7 shows the equilibrium amplitude of the least stable mode, $\overline{B_1}(k) = \varepsilon \Delta k |B_1(k, n = 0)|$, obtained by solving equation (43). As might be anticipated from the results in Table 5, the amplitudes of the first eigenmode for the mean flow distortion ($k = 0$) predicted by the two computations do not agree. The amplitudes of the least stable mode for the fundamental wave $k = 0.75$ predicted by the two computations, however, differ only by 13.3%.

Table 6. Nonlinear terms for the different eigenmodes for $Ra = 200$ and $k = 0.75$

m	$k = 0$	$k = 0.75$	$k = 1.5$
1	0.1674E−04	−0.9466E−05	0.1141E−05
2	0.1827E−04	0.1346E−07	0.1204E−08
3	0.1827E−04	0.9212E−05	0.2070E−05
4	0.5317E−04	0.1862E−05	0.1346E−04
5	0.1757E−04	0.2538E−04	0.1380E−06
6	0.1038E−04	0.1644E−04	0.1311E−04
7	0.1189E−04	0.2102E−04	0.1871E−05
8	0.3753E−05	0.4755E−04	0.6754E−05
9	0.1904E−05	0.4583E−04	0.9962E−05
10	0.1241E−04	0.7208E−05	0.5803E−05
11	0.1901E−05	0.9794E−05	0.1956E−04
12	0.6267E−06	0.3103E−05	0.9016E−05
13	0.5627E−06	0.3569E−05	0.2434E−05
14	0.4698E−06	0.7030E−06	0.1481E−04
15	0.8140E−07	0.1956E−06	0.4349E−05
16	0.1092E−06	0.3942E−05	0.4483E−05
17	0.1449E−05	0.7322E−07	0.8563E−06
18	0.1105E−06	0.5029E−08	0.1212E−06
19	0.1934E−07	0.2480E−07	0.1674E−05
20	0.2816E−07	0.5013E−06	0.1004E−06

Table 8 shows the amplitudes of the various eigenmodes for the equilibrium state shown in Fig. 2(b). The corresponding nonlinear terms are shown in

Table 7. Amplitudes of least stable eigenmode for $Ra = 200$ and $k = 0.75$ predicted by the weakly nonlinear formulation

k	0	0.75	1.5
$\bar{B}_1(k)$	0.3471E−01	0.3892E−02	0.4396E−03

Table 8. Amplitudes of the different eigenmodes for $Ra = 200$ and $k = 0.25$

m	$k = 0$	$k = 0.5$	$k = 1$
1	0.1078E−01	0.5596E−02	0.1005E−02
2	0.6516E−02	0.1358E−04	0.7699E−06
3	0.6516E−02	0.3368E−03	0.8185E−03
4	0.9105E−02	0.4795E−03	0.3209E−03
5	0.1723E−02	0.1364E−02	0.2670E−04
6	0.5675E−03	0.1975E−02	0.3587E−03
7	0.4829E−03	0.6819E−03	0.1961E−03
8	0.1635E−03	0.9276E−03	0.7020E−04
9	0.3080E−04	0.3743E−03	0.5065E−03
10	0.3155E−03	0.2070E−03	0.3535E−03
11	0.1914E−04	0.3555E−04	0.5937E−04
12	0.7851E−05	0.1044E−04	0.8617E−04
13	0.4032E−05	0.4293E−04	0.1620E−04
14	0.3797E−05	0.1773E−05	0.1570E−04
15	0.3246E−06	0.4192E−06	0.3354E−05
16	0.4966E−06	0.2273E−04	0.1970E−04
17	0.7874E−05	0.2217E−06	0.6953E−06
18	0.4024E−06	0.2808E−07	0.4933E−07
19	0.5556E−07	0.3098E−07	0.2303E−07
20	0.8655E−07	0.3378E−05	0.6783E−05

Table 9. Nonlinear terms for the different eigenmodes for $Ra = 200$ and $k = 0.25$

m	$k = 0$	$k = 0.5$	$k = 1$
1	0.1325E−01	−0.1131E−04	−0.8440E−06
2	0.1912E−04	0.4243E−07	0.3782E−08
3	0.1912E−04	0.3833E−05	0.1212E−04
4	0.4865E−04	0.6023E−05	0.5694E−05
5	0.1752E−04	0.2817E−04	0.5190E−06
6	0.9469E−05	0.4107E−04	0.1027E−04
7	0.9208E−05	0.1789E−04	0.6520E−05
8	0.4065E−05	0.3056E−04	0.2849E−05
9	0.1069E−05	0.1676E−04	0.2300E−04
10	0.1390E−04	0.9339E−05	0.1941E−04
11	0.8849E−06	0.2063E−05	0.3571E−05
12	0.4661E−06	0.7629E−06	0.6017E−05
13	0.2991E−06	0.3376E−05	0.1266E−05
14	0.2986E−06	0.1590E−06	0.1367E−05
15	0.2942E−07	0.4524E−07	0.3546E−06
16	0.5398E−07	0.2705E−05	0.2319E−05
17	0.9697E−06	0.2833E−07	0.8752E−07
18	0.5168E−07	0.4192E−08	0.7280E−08
19	0.8322E−08	0.5342E−08	0.3948E−08
20	0.1496E−07	0.5974E−06	0.1191E−05

Table 11. Amplitudes of the different eigenmodes for $Ra = 100$

m	$k = 0$	$k = 0.3$	$k = 0.6$
1	0.4498E−02	0.2808E−02	0.2172E−03
2	0.2186E−02	0.7416E−06	0.2843E−07
3	0.2186E−02	0.5678E−04	0.1283E−03
4	0.2139E−02	0.5499E−04	0.2907E−05
5	0.1766E−03	0.6950E−04	0.3235E−04
6	0.1126E−03	0.4443E−04	0.2028E−04
7	0.6997E−04	0.5189E−04	0.1013E−04
8	0.2145E−04	0.1292E−04	0.1999E−04
9	0.4160E−05	0.1783E−04	0.6593E−05
10	0.3896E−04	0.3883E−05	0.6824E−05
11	0.2224E−05	0.6629E−06	0.9856E−06
12	0.5400E−06	0.1970E−06	0.2501E−06
13	0.3262E−06	0.2622E−05	0.3327E−05
14	0.3756E−06	0.8883E−08	0.5294E−07
15	0.5166E−07	0.1160E−07	0.2127E−07
16	0.2441E−07	0.1250E−05	0.2173E−05
17	0.9859E−06	0.3021E−08	0.6756E−08
18	0.1894E−07	0.8179E−09	0.1637E−08
19	0.3403E−08	0.1228E−08	0.1166E−08
20	0.4740E−08	0.2404E−06	0.9549E−06

Table 12. Nonlinear terms for the different eigenmodes for $Ra = 100$

m	$k = 0$	$k = 0.3$	$k = 0.6$
1	0.3456E−05	−0.6679E−06	0.2216E−06
2	0.6752E−05	0.3038E−08	0.1880E−09
3	0.6752E−05	0.5319E−06	0.1524E−05
4	0.1109E−04	0.6834E−06	0.6372E−07
5	0.1781E−05	0.1176E−05	0.7232E−06
6	0.1873E−05	0.1031E−05	0.4612E−06
7	0.1354E−05	0.1241E−05	0.3206E−06
8	0.5329E−06	0.4309E−06	0.6679E−06
9	0.1444E−06	0.7557E−06	0.2829E−06
10	0.1721E−05	0.1752E−06	0.3423E−06
11	0.1028E−06	0.3874E−07	0.5514E−07
12	0.3206E−07	0.1446E−07	0.1780E−07
13	0.2419E−07	0.2052E−06	0.2550E−06
14	0.2959E−07	0.7994E−09	0.4668E−08
15	0.4681E−08	0.1255E−08	0.2267E−08
16	0.2653E−08	0.1491E−06	0.2584E−06
17	0.1215E−06	0.3867E−09	0.8557E−09
18	0.2433E−08	0.1222E−09	0.2428E−09
19	0.5099E−09	0.2119E−09	0.2001E−09
20	0.8193E−09	0.4254E−07	0.1680E−06

Table 9. The initial disturbance used in this computation consisted of a single dominant mode with wavenumber $k = 0.25$. This mode decayed and its harmonic $k = 0.5$ became the dominant wavenumber in the equilibrium state. Table 10 shows the corresponding results predicted by equation (43). In the latter computation, the initial mode $k = 0.25$ remained the dominant mode in the final equilibrium state. Thus, the two computations do not agree even qualitatively for this case.

Tables 11–13 show the results of computations done at a lower Rayleigh number $Ra = 100$ with initial

Table 10. Amplitudes of least stable eigenmode for $Ra = 200$ and $k = 0.25$ predicted by the weakly nonlinear formulation

k	0	0.25	0.5
$\bar{B}_1(k)$	0.4782E−01	0.7072E−02	0.3284E−02

Table 13. Amplitudes of least stable eigenmode for $Ra = 100$ predicted by the weakly nonlinear formulation

k	0	0.3	0.6
$\bar{B}_1(k)$	0.2766E−02	0.2523E−02	0.3767E−03

Table 14. Amplitudes of the different eigenmodes for $Ra = 90$

m	$k = 0$	$k = 0.3$	$k = 0.6$
1	0.3003E−03	0.6779E−03	0.1348E−04
2	0.6671E−03	0.7655E−08	0.1100E−08
3	0.7364E−03	0.1106E−05	0.6946E−05
4	0.1388E−03	0.7318E−06	0.1852E−05
5	0.9956E−05	0.7898E−06	0.9454E−06
6	0.6901E−05	0.5734E−06	0.1073E−06
7	0.4321E−05	0.6653E−06	0.5424E−06
8	0.1250E−05	0.1908E−06	0.9596E−06
9	0.2711E−06	0.2902E−06	0.5562E−06
10	0.2225E−05	0.5848E−07	0.4356E−06
11	0.1538E−06	0.1068E−07	0.6340E−07
12	0.3224E−07	0.2844E−08	0.4877E−08
13	0.2194E−07	0.4087E−07	0.2512E−06
14	0.2747E−07	0.2944E−10	0.1299E−08
15	0.3478E−08	0.1886E−09	0.8276E−09
16	0.1418E−08	0.1983E−07	0.1251E−06
17	0.6012E−07	0.5279E−10	0.3683E−09
18	0.1108E−08	0.1745E−10	0.7801E−10
19	0.1989E−09	0.2700E−10	0.8881E−10
20	0.2692E−09	0.3272E−08	0.5811E−07

Table 15. Nonlinear terms for the different eigenmodes for $Ra = 90$

m	$k = 0$	$k = 0.3$	$k = 0.6$
1	0.2132E−06	−0.1029E−07	0.2323E−07
2	0.1986E−05	0.3405E−10	0.7914E−11
3	0.2386E−05	0.1033E−07	0.8261E−07
4	0.7172E−06	0.9721E−08	0.4267E−07
5	0.1003E−06	0.1322E−07	0.2196E−07
6	0.1148E−06	0.1349E−07	0.2516E−08
7	0.8375E−07	0.1592E−07	0.1719E−07
8	0.3105E−07	0.6336E−08	0.3349E−07
9	0.9405E−08	0.1231E−07	0.2362E−07
10	0.9833E−07	0.2631E−08	0.2206E−07
11	0.7104E−08	0.6228E−09	0.3526E−08
12	0.1914E−08	0.2085E−09	0.3454E−09
13	0.1627E−08	0.3194E−08	0.1907E−07
14	0.2164E−08	0.2647E−11	0.1141E−09
15	0.3152E−09	0.2040E−10	0.8804E−10
16	0.1541E−09	0.2365E−08	0.1488E−07
17	0.7407E−08	0.6754E−11	0.4657E−10
18	0.1424E−09	0.2607E−11	0.1156E−10
19	0.2979E−10	0.4657E−11	0.1523E−10
20	0.4653E−10	0.5788E−09	0.1022E−07

conditions consisting of a single dominant mode with wavenumber $k = 0.3$, which is the critical wavenumber. This mode remained the dominant wavenumber in the final equilibrium state. Table 11 shows that the least stable eigenmode for the fundamental wavenumber $k = 0.3$ is indeed the dominant eigenmode for this wave, as predicted by classical weakly nonlinear theories; the amplitudes of the higher eigenmodes for $k = 0.3$ are much smaller than the amplitude of the first mode. However, the amplitude of the least stable eigenmode for $k = 0$ is higher than the amplitude of the least stable eigenmode for the fundamental wave $k = 0.3$. Nonlinear interactions excite a number of eigenmodes for the mean flow distortion ($k = 0$) and the second harmonic ($k = 0.6$), as indicated by Table 12. The weakly nonlinear prediction for this case is shown in Table 13. The difference between the amplitudes of the least stable eigenmode for the fundamental wave predicted by the two computations is 10.3% at this Rayleigh number. However, the corresponding amplitudes for $k = 0$ still do not agree.

Tables 14–16 present the results obtained at $Ra = 90$ which is very close to the critical Rayleigh number $Ra_c = 89$. Table 14 shows that the least stable eigenmode for the fundamental wave $k = 0.3$ is the dominant eigenmode for this wave, as in the case of $Ra = 100$. A glance at Table 16 reveals that the prediction of the weakly nonlinear computation for the amplitude of this eigenmode is within 2.3% of the result predicted by the numerical solution of equation (15). However, the 2nd and 3rd eigenmodes for $k = 0$ in this case have amplitudes higher than the amplitude of the least stable eigenmode for $k = 0$.

Table 17 compares the average Nusselt numbers predicted by the numerical solution of equation (15) and equations (18) at $Ra = 90$, 100 and 200. The average Nusselt number is defined by

$$Nu = \frac{1}{\lambda}\int_0^{\lambda} Nu_z \, dz$$

where $\lambda = 2\pi/k_f$, k_f is the wavenumber of the dominant wave in the final equilbrium state, $Nu_z = hd/k$ is the local Nusselt number, $\bar{k}$ is the thermal conductivity of the fluid, $h = q_w/T_w - T_b$ is the local heat-transfer coefficient, q_w and T_w are the local heat-flux and temperature of the inner wall, respectively, and T_b is the bulk temperature of the fluid. The Nusselt numbers for different initial conditions is presented in Table 17. The wavenumber of the initial disturbance is denoted by k_i in Table 17, and the Nusselt number predicted by the weakly nonlinear computation is denoted by Nu_{WNL}. The Nusselt numbers predicted by the two computations are closer than might be expected from the detailed comparison of the amplitudes for the various eigenmodes presented in Tables

Table 16. Amplitudes of least stable eigenmode for $Ra = 90$ predicted by the weakly nonlinear formulation

k	0	0.3	0.6
$\bar{B}_i(k)$	0.2104E−03	0.6623E−03	0.2114E−04

Table 17. Comparison of the Nusselt numbers predicted by the fully nonlinear numerical solution and the weakly nonlinear formulation

Ra	90	100	200	200
k_i	0.3	0.3	0.75	0.25
Nu	3.8322	3.9479	4.8132	4.7436
Nu_{WNI}	3.8324	3.9416	4.7322	4.7828

5–16. The maximum error in the prediction of the Nusselt number is 1.7% and occurs at $Ra = 200$. The Nusselt numbers predicted at $Ra = 90$ by the two computations differ only by 0.005%. This implies that the prediction of weakly nonlinear theories for global quantities such as the Nusselt number is quite good in a parameter range near the neutral curve of linear stability, although the details of the flow field predicted by these theories do not agree with a numerical solution of the Navier–Stokes equations. Table 17 also illustrates that the equilibrium Nusselt number is not a unique function of the dynamic similarity parameters. Table 17 presents two possible equilibrium states of the flow at $Ra = 200$, with different Nusselt numbers. We did not carry out an exhaustive search for all possible equilibrium states to find the true uncertainty in the Nusselt number. From the few cases we computed, we found a 10% uncertainty in the Nusselt number at $Ra = 200$.

4. CONCLUSIONS

The integrodifferential equation (15) for the amplitude density function of a continuous spectrum has been shown to be equivalent to the Navier–Stokes equations. The equation (15) has been approximated by a perturbation expansion with multiple time scales. This yields equation (43), which describes the weakly nonlinear interactions among the wave components of a continuous spectrum of travelling waves. The perturbation expansion demonstrates that the important cases of monochromatic waves and wavepackets are special limiting cases of the integro-differential equation (43).

The Ginzburg–Landau equation of classical weakly nonlinear theories describing the evolution of the envelope of slowly-varying wavepackets, which is often used to study spatio-temporal chaos, is shown to be valid only locally near the onset of linear instability. This implies that chaotic solutions of this equation may not have physical relevance in a parameter range which is far from the neutral curve of linear stability. Furthermore, the solutions of this equation can only describe a slow spatial modulation of a periodic fluid motion with a single dominant wavenumber, and is incapable of describing chaotic fluid motion with a general spatial variation. On the other hand, solutions of the integro-differential equation (15) are valid for all parameters, include full spectra and can describe chaotic fluid motions properly.

Numerical results demonstrate that linearization in the weakly nonlinear instability theories is a good approximation since the values of amplitude functions are usually very small. However, using only one eigenfunction, associated with the least stable or most unstable eigenvalue, in the expansion of weakly nonlinear theories is insufficient. This is because that energy is transfered nonlinearly into higher eigenmodes to balance out the larger dissipation rate, associated with the larger value of ω_m^1. One may visualize intuitively that eigenfunctions represent eddies of different sizes along r directions. The higher eigenmodes correspond to eddies of smaller sizes which have larger dissipation rates. We found the numerical results diverge due to lack of dissipation when number of eigenmodes used in the expansion is too small. The numerical solution of equation (43) requires the evaluation of two integrals. The first integral involves a quadratic nonlinearity, while the second involves a cubic nonlinearity. The solution of equation (15), on the other hand, requires the evaluation of only one integral involving a quadratic nonlinearity. For the same accuracy the weakly nonlinear theories require, at least, double storage and CPU time than a direct solution of the nonlinear formulation, (15). Moreover, the numerical solution of equation (15) is an exact solution of the Navier–Stokes equations. Thus, from computational point of view, it is preferable to solve equations (15) directly.

The eigenfunction expansion used in the current formulation requires only one amplitude density function for the all dependent variables, such as velocity components and temperature. This substantially simplifies the final form of the governing equations (15). Therefore, the required CPU time to solve the integro-differential equations is much less than a spectral method employing Fourier–Chebyshev functions, or other functions in solving the Navier–Stokes equations. The current formulation provides a new efficient algorithm for the solution of the Navier–Stokes equations, and can be used for the direct simulation of turbulent flows which are homogeneous in two directions. The extension of the formulation to fluid dynamical problems without this limitation is straightforward.

Another interesting result is that the equilibrium state of the mean flow and the wave components is not unique after the first bifurcation point, but depends on the waveform of the initial disturbance. This may imply that time-averaged turbulent mean flows do not have to be unique for a given value of the dynamic similarity parameters, such as the Reynolds number. Consequently, the ergodic hypothesis does not hold. Thus, the values of time-averaged turbulent statistical quantities are not necessarily equal to the ensemble average even for stationary turbulence. The ensemble average would be the averaged value of the all possible time averages which can be measured independently. From an application point of view, only time average has physical significance.

Acknowledgement—The results of the paper were computed by Cray C90 at the Pittsburgh Supercomputing Center. Their quick approval of the grant, CTS930015P, and their efficient support made the computation possible and is acknowledged.

REFERENCES

1. J. T. Stuart, On the non-linear mechanics of wave disturbances in stable and unstable parallel flows, Part 1, *J. Fluid Mech.* **9**, 353–370 (1960).

2. J. Watson, On the non-linear mechanics of wave disturbances in stable and unstable parallel flows, Part 2, *J. Fluid Mech.* **9,** 371–389 (1960).
3. K. Stewartson and J. T. Stuart, A non-linear instability theory for a wave system in plane–Poiseuille flow, *J. Fluid Mech.* **48,** 529–545 (1971).
4. A. C. Newell and J. A. Whitehead, Finite bandwidth, finite amplitude convection, *J. Fluid Mech.* **38,** 279–303 (1969).
5. L. A. Segel, Distant side-walls cause slow amplitude modulation of cellular convection, *J. Fluid Mech.* **38,** 203–224 (1969).
6. L. S. Yao, Is fully-developed and non-isothermal flow possible in a vertical pipe? *Int. J. Heat Mass Transfer* **30,** 707–716 (1987).
7. L. S. Yao, Linear stability analysis for opposing mixed convection in a vertical pipe, *Int. J. Heat Mass Transfer* **30,** 810–811 (1987).
8. L. S. Yao and B. B. Rogers, The linear stability of mixed-convection in a vertical annulus, *J. Fluid Mech.* **201,** 279–298 (1989).
9. L. S. Yao and B. B. Rogers, Mixed convection in an annulus of large aspect ratio, *J. Heat Transfer* **111,** 683–689 (1989).
10. L. S. Yao and B. B. Rogers, Finite-amplitude instability of non-isothermal flow in a vertical annulus, *Proc. R. Soc. Lond. A* **437,** 267–290 (1992).
11. B. B. Rogers, S. Ghosh Moulic and L. S. Yao, Finite-amplitude instability of mixed-convection, *J. Fluid Mech.* **254,** 229–250 (1993).
12. L. S. Yao and S. Ghosh Moulic, Uncertainty of convection, *Int. J. Heat Mass Transfer* **37,** 1713–1721 (1994).
13. L. S. Yao and S. Ghosh Moulic, Taylor–Couette instability with a continuous spectrum, *J. Appl Mech.* (in press).
14. T. J. Hanratty, E. M. Rosen and R. L. Kabel, Effect of heat transfer on flow field at low Reynolds numbers in vertical tubes, *Ind. Engng Chem.* **50,** 815–820 (1958).
15. G. A. Kemeny and E. V. Somers, Combined free and forced convective flow in vertical circular tubes—experiments with water and oil, *J. Heat Transfer* **84,** 339–346 (1962).
16. G. F. Scheele and T. J. Hanratty, Effect of natural convection on stability of flow in a vertical pipe, *J. Fluid Mech.* **14,** 244–256 (1962).
17. D. Maitra and K. S. Raju, Combined free and forced convection laminar heat transfer in a vertical annulus, *J. Heat Transfer* **97,** 135–137 (1975).
18. J. T. Stuart and R. C. DiPrima, The Eckhaus and Benjamin–Feir resonance mechanisms, *Proc. R. Soc. A* **362,** 27–41 (1978).
19. H. A. Snyder, Wave-number selection at finite amplitude in rotating Couette flow, *J. Fluid Mech.* **35,** 273–298 (1969).
20. J. E. Burkhalter and E. L. Koschmieder, Steady supercritical Taylor vortex flow, *J. Fluid Mech.* **58,** 547–560 (1973).
21. J. E. Burkhalter and E. L. Koschmieder, Steady supercritical Taylor vortices after sudden starts, *Phys. Fluids* **17,** 1929–1935 (1974).
22. O. Haupt, Uber die Entwicklung einer willkurlichen Funkton nach den Eigenfunktionen des Turbulenzproblems, *Sber. bayer. Akad. Wiss.* **2,** 289 (1912).
23. I. V. Schensted, Contributions to the theory of hydrodynamic stability, Ph.D. Dissertation, University of Michigan (1960).
24. R. C. DiPrima and G. J. Habetler, A completeness theorem for non-selfadjoint eigenvalue problems in hydrodynamic stability, *Arch. Rat. Mech. Anal.* **34,** 218–227 (1969).
25. C. E. Grosch and H. Salwen, The continuous spectrum of the Orr–Sommerfeld equation. Part 1. The spectrum and the eigenfunctions, *J. Fluid Mech.* **87,** 33–54 (1978).
26. B. Friedman, *Principles and Techniques of Applied Mathematics.* Wiley, New York (1956).
27. R. T. Gregory, Defective and derogatory matrices, *SIAM Rev.* **2,** 134–139 (1960).
28. F. Brauer and J. A. Nohel, *The Qualitative Theory of Ordinary Differential Equations. An Introduction.* Dover Publications, New York (1969).
29. K. Nozaki and N. Bekki, Pattern selection and spatio-temporal transition in chaos in the Ginzburg–Landau equation, *Phy. Rev. Lett.* **51,** 2171–2174 (1983).
30. H. T. Moon, P. Huerre and L. G. Redekopp, Three-frequency motion and chaos in the Ginzburg–Landau equation, *Phy. Rev. Lett.* **49,** 458–460 (1982).
31. Y. Kuramoto and T. Yamada, Turbulent state in chemical reactions, *Prog. Theor. Phys.* **56,** 679–681 (1976).
32. L. Kleiser and U. Schumann, Treatment of incompressibility and boundary conditions in three-dimensional numerical spectral simulations of plane channel flows, *Proceedings of the 3rd GAMM Conference on Numerical Methods in Fluid Mechanics* (Edited by E. H. Hirschel), pp. 165–173. Vieweg, Braunschweig (1980).
33. A. D. D. Craik, Nonlinear resonant instability in boundary layers, *J. Fluid Mech.* **50,** 393–413 (1971).
34. J. R. Usher and A. D. D. Craik, Nonlinear wave interactions in shear flows—II. Third order theory, *J. Fluid Mech.* **70,** 437–461 (1975).
35. D. J. Benney and A. C. Newell, The propagation of nonlinear wave envelopes, *J. Math. Phys.* **46,** 133–139 (1967).
36. S. Ghosh Moulic and L. S. Yao, Taylor–Couette instability with a continuous spectrum—II. Travelling waves, in preparation.